Anonymous Referee #1

General comments

The authors present an experimental study of aerosols collected from Hainan Island, South China. The analysis includes absorption coefficients, mass concentrations of black carbon, organic carbon, inorganic elements, and water-soluble cations and anions. Major findings include the source apportionment of the total absorption coefficient and contribution to radiative forcing. The study shows the importance of considering ship emissions in forcing calculation. Overall, the manuscript presents interesting data and analysis shows merit.

Response: We thank the reviewer for his/her valuable suggestions, and it is useful for improving our manuscript. We have made modifications accordingly based on the reviewer's comments. Below are point-to-point responses.

Specific comments

1. This study uses AE-33 and PAX to measure absorption. AE-33 provides the mass of absorbing aerosols as final products. Previous studies have reported the calculation of absorption coefficients from AE-33 mass concentration. However, for the sake of completeness, I would recommend to include those steps in supplementary.

Response: We followed the reviewer's suggestion and added the following in the revised manuscript:

> "Since the AE33 aethalometer records the BC mass concentrations, the Abs(λ) at each wavelength were retrieved by getting the product of BC mass concentration ([BC]) and mass absorption cross-section (MAC) used in the instrument (Abs(λ) = [BC] × MAC) (Drinovec et al., 2015)."

2. This study used a Nafion dryer to reduce the RH of particles collected. These dryers are known to minimize particle concentration during the drying process. Is there any data on the % of particle loss within the dryer?

Response: We conducted a test to compare the measured light absorption coefficients

(Abs(λ)) with and without the Nafion tube. As shown in Fig. R1 below (also see Fig. S2 in the revised supporting information), the loss of Abs(λ) is little and can be ignored. We have added a sentence to show the result of this test in the revised manuscript. It reads as follows:

"As shown in Fig. S2, the loss of Abs(λ) caused by the dryer was ignored."

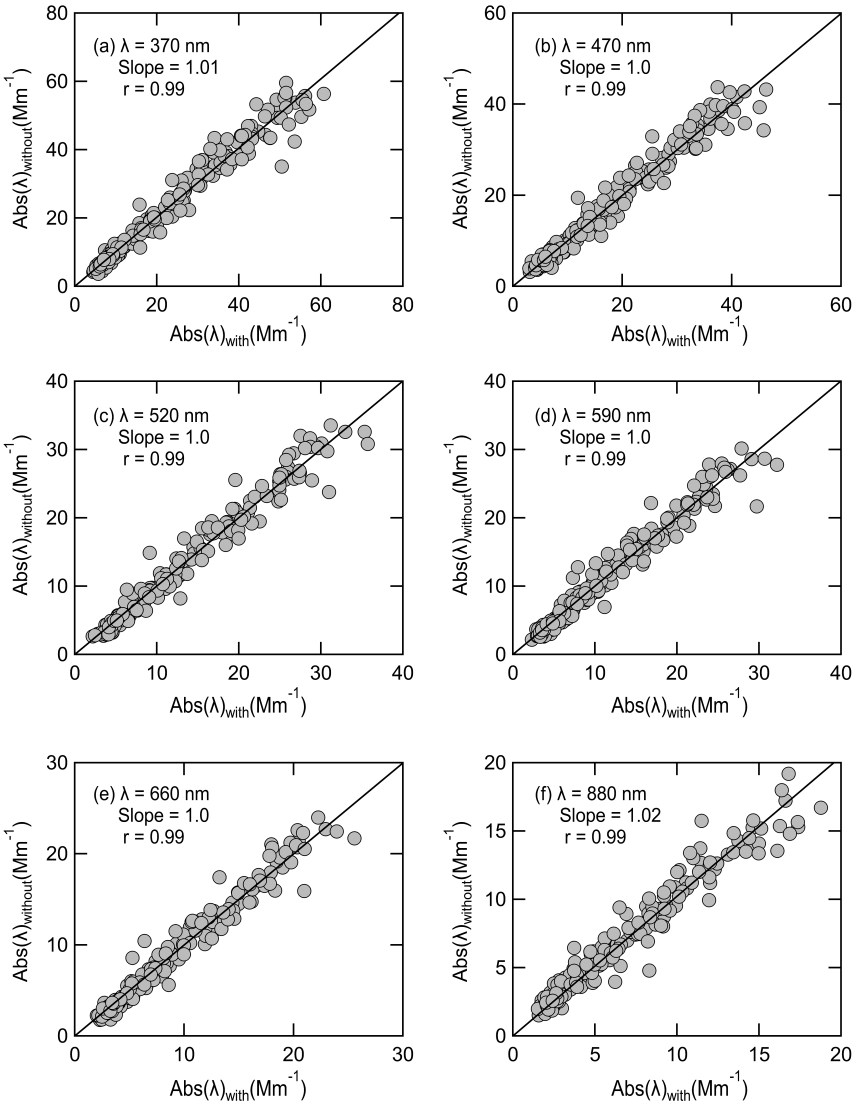

Figure R1. Scatter plot of light absorption coefficient measured with ($Abs(\lambda)_{with}$) and without ($Abs(\lambda)_{without}$) Nafion dryer (MD-700-24S-3). λ is the wavelength of 370, 470, 520, 590, 660, or 880 nm.

3. The Nafion dryers were connected to Aethalometers only? Aethalometer data is less susceptible to RH. But the PAX data can be influenced by high RH. Was there a dryer

connected to PAX?

Response: The PAX and AE33 share a same sampling tube and was set in parallel with a tee. Therefore, the PAX and AE33 were both dried by the Nafion dryer. We have clarified and added the following information in the revised manuscript:

> "It was set in parallel with the AE33 aethalometer using the same $PM_{2.5}$ cyclone and Nafion® dryer."

4. There was a $PM_{2.5}$ cyclone for Aethalometer and no cyclone for PAX. I remember the penetration efficiency of PAX reduces drastically after 1 micrometer. So, both instruments were measuring different size-cutoff particles.

Response: We apologize for our unclear description. As replied above, the PAX and AE33 were both collected the ambient aerosols using the same $PM_{2.5}$ cyclone. Therefore , the same size range of particles was measured by the PAX and AE33.

5. What is the area of quartz filters used?

Response: The area of quartz filter is 8 × 10 inch. We have added this information in the manuscript. It now reads as follows:

> "The $PM_{2.5}$ quartz-fiber filters (8 × 10 inch) (QM/A; GE Healthcare, Chicago, IL, USA) were collected during the day (from 08:00 to 20:00) and at night (from 20:00 to 08:00 the next day) using a high-volume air sampler (Tisch Environmental, Inc., USA) with a flowrate of 1.13 m^3 min^{-1}."

6. What is the flow rate of the high-volume sampler?

Response: The flowrate of high-volume sampler was 1.13 m^3 min^{-1}. We have added this information in the manuscript as shown above response.

7. One major shortcoming in this study is the absence of 'lensing effect' while calculating absorption. Studies have shown that the lensing effect can contribute to significant absorption. Since Aethalometer uses a filter tape to collect particles, one can

assume the core-shell structure of particles (the reason for lensing effect) gets destroyed. But the absorption from PAX will have contributions from the lensing effect. The slope of 2.29 in Figure S3 might include the lensing effect. Since the experimental setup used in this study does not measure the absorption of core-shell and core separately, it will be difficult to distinguish the contribution from the lensing effect. I would suggest the authors include this possibility in text.

Response: We thank the reviewer for explanation the impact of 'lensing effect' on comparison of PAX and AE33. In the revised manuscript, we have added this possible effect:

> "A slope of 2.3 was regarded as the correction factor and was comparable to the values of 2.0–2.6 reported by previous studies using a similar method (Qin et al., 2018; Tasoglou et al., 2017; Wang et al., 2019b). This difference may mainly be related to the matrix scattering and lensing effects."

8. Figure 1a – shows the apportionment of Abs, and the same is repeated as Figure 1b. Removing the repeated portion from 1a would give better visibility to it.

Response: We followed the reviewer's suggestion and modified this figure as shown in Fig. R2 below (also see Fig. 3 in the revised manuscript).

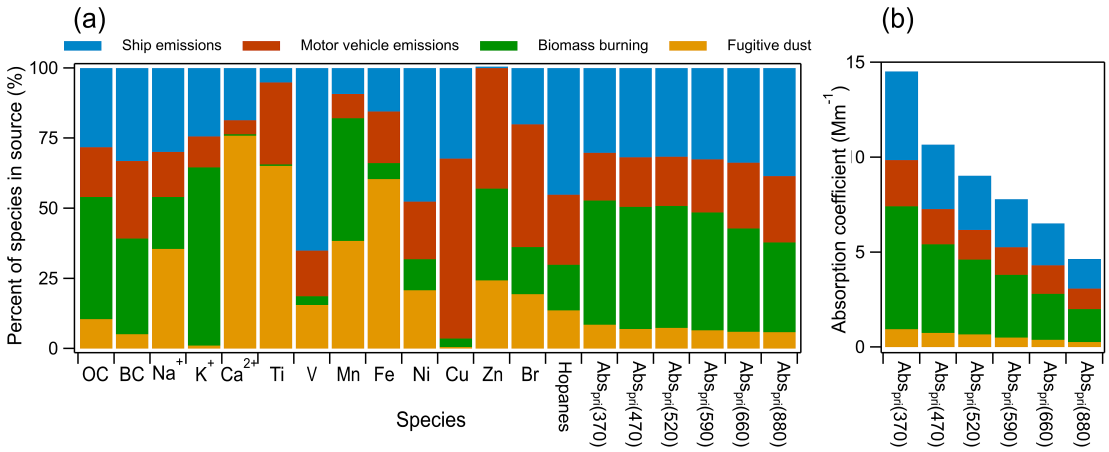

Figure R2. (a) Contributions of the four sources to each species from the positive matrix factorization model and (b) the light absorption of primary aerosols from each source at different wavelengths ($Abs_{pri}(\lambda)$, λ = 370, 470, 520, 590, 660, and 880 nm)

during the study.

9. Page 2, line 13- Optical properties of LAC is not just related to its source. It also depends on the atmospheric conditions and secondary processing.

Response: We agree with the reviewer and revised the original sentence to:

> "The optical properties of LAC aerosols are closely related to their sources as well as atmospheric conditions and secondary processing."

10. Page 4, line 3 – Educational and residential areas will have their pollution sources such as vehicles, cooking, etc.

Response: We agree with the reviewer. In the revised manuscript, we have revised the original description to:

> "The sampling site is predominantly an educational and residential area with typical urban sources of emission including vehicles and cooking appliances."

11. Page 5, Paragraph 1 – The whole paragraph is about the analysis of filters collected. It must be specified initially.

Response: Following the reviewer's suggestion, we have added a sentence to clarify this in the revised manuscript:

> "The collected quartz-fiber filters were used to analyse inorganic elements, carbonaceous matter, water-soluble ions, and organics."

12. Page 7, line 4 – Which PMF system was used for the analysis? I guess US EPA PMF 5.0! It needs to be mentioned with a reference.

Response: Yes, the version of PMF5.0 from US EPA was used in our study. We have added this information in the revised manuscript. It now reads as follows:

> "The PMF version 5.0 (PMF5.0) from the US Environmental Protection Agency (Norris et al., 2014) was applied to determine the contribution of various sources

to aerosol light absorption."

13. Page 9, line 24 – Error bars on Y-axis needed. Since the X-axis is from filters (12-hour sample) and the Y-axis is the average of the same from AE-33 Abs, the error bars are required to see the spread of data.

Response: We followed the reviewer's suggestion, and the revised version is shown in Fig. R3 and Fig. R4 below (also see Fig. S5 and Fig. S6 in the revised supporting information).

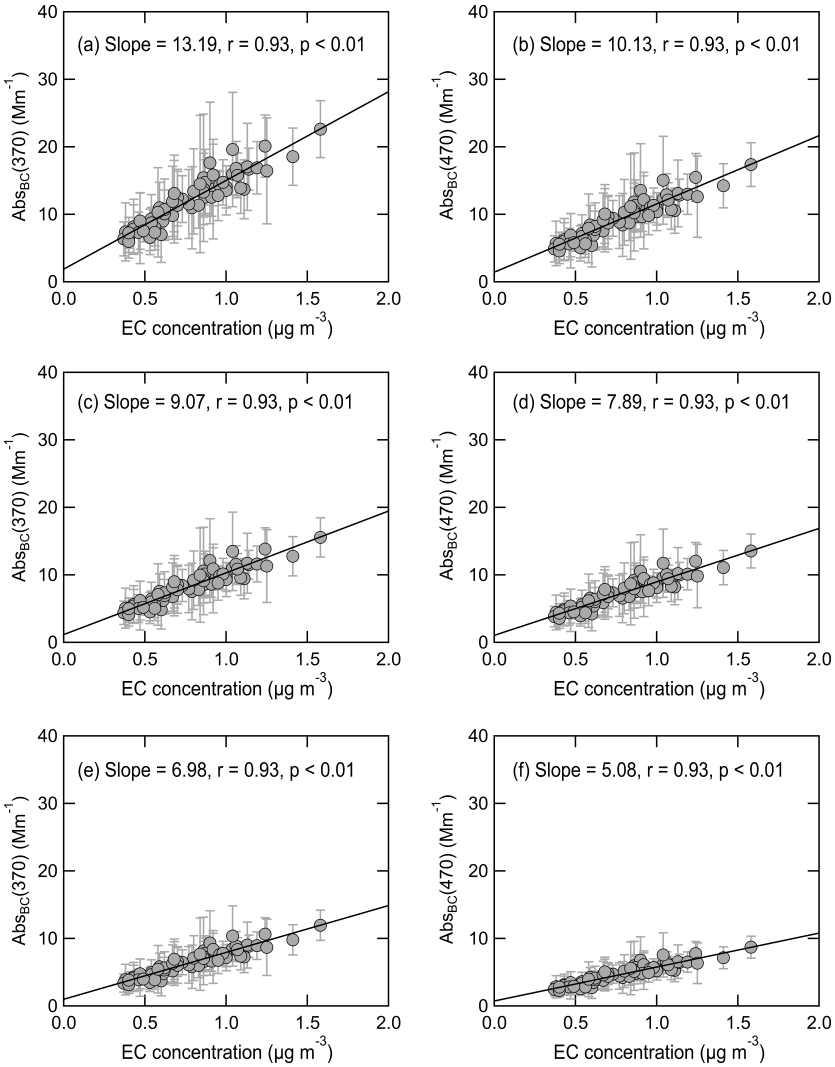

Figure R3. Scatter plots of light absorption of black carbon at different wavelengths ($Abs_{BC}(\lambda)$, λ = 370, 470, 520, 590, 660, and 880 nm) versus mass concentration of elemental carbon (EC). The black lines are the linear regression. The vertical error bars represent one standard deviation of $Abs_{BC}(\lambda)$.

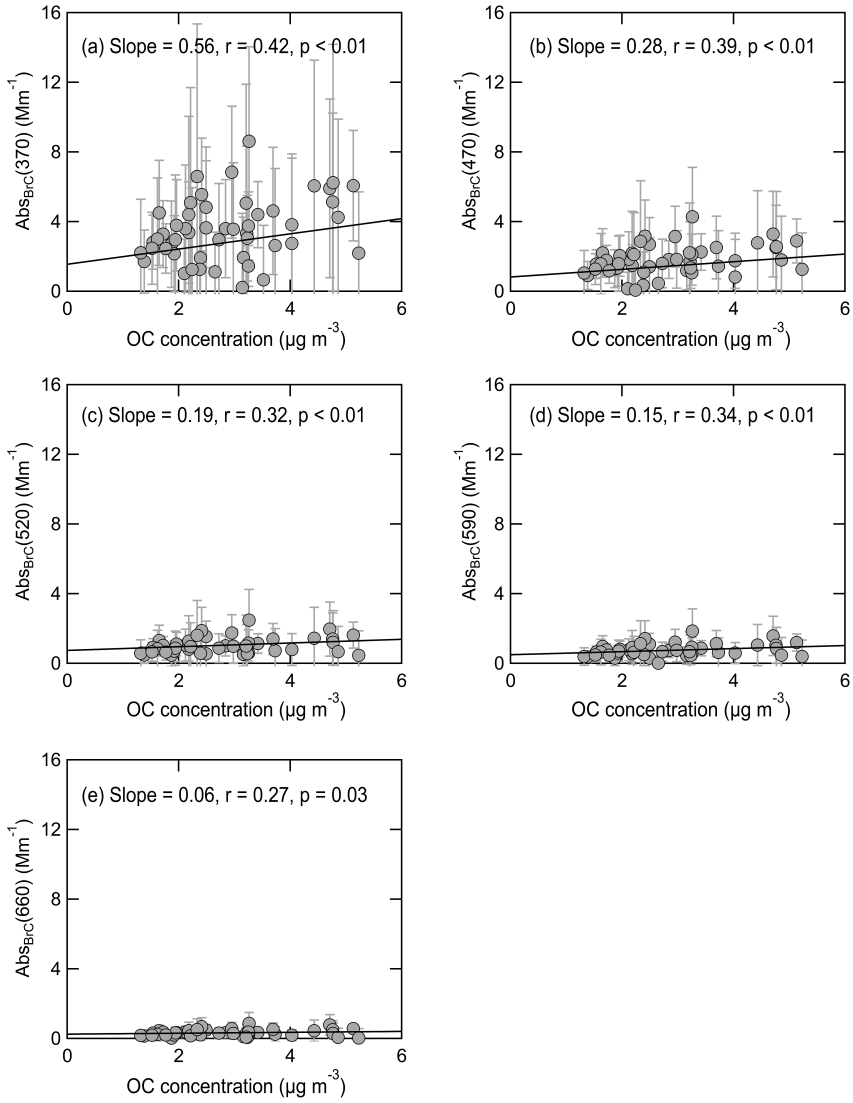

Figure R4. Scatter plots of light absorption of brown carbon at different wavelengths ($Abs_{BrC}(\lambda)$, λ = 370, 470, 520, 590, and 660 nm) versus mass concentration of organic carbon (OC). The black lines are the linear regression. The vertical error bars represent one standard deviation of $Abs_{BrC}(\lambda)$.

14. Page 12, line 1 – The cluster 2 back trajectory doesn't touch the Vietnam cost to influence the biomass burning. Was there a spread towards land for this cluster?

Response: Thanks for the reviewer pointing out this issue. In the revised manuscript, we reworked this paragraph to avoid any misunderstanding. It now reads as follows:

"Cluster #2 originated from the South China Sea near the Indochina Peninsula and accounted for 35% of the total trajectories. The $Abs_{ship}(\lambda)$ was also vital in

this cluster, accounting for 34–37% of $Abs_{pri}(\lambda)$. Fig. S10 shows that the $Abs_{pri}(\lambda)$ of Cluster #2 displayed a similar diurnal trend as that of Cluster #1. Considering that the air masses of Cluster #2 also originated from the South China Sea, the sources except for ship emissions were mainly influenced by local discharge."

Technical corrections

15. Page 2, line 26 – Don't use 'firstly'. 'First' is fine.

Response: Change made.

16. Page 4, line 10 – 'As described previously' – It is not described anywhere before.

Response: This sentence has been revised to "Afterwards, seven light emitting diodes (λ = 370, 470, 520, 590, 660, 880, and 950 nm) in the AE33 aethalometer were used to irradiate the filter deposition spot to obtain light attenuation as previously described (Drinovec et al., 2015)."

Anonymous Referee #2

This study performed ground measurements in a small city at the very south end of continental China along the South China Sea. The authors attempted to attribute the sources from the composition and absorption measurements using receptor models, however the analysis of the entire study is rough and the conclusions are vague for the current version.

Response: The authors appreciate the reviewer's valuable suggestions, and we believe that the revised manuscript has been significantly improved after considering the comments. Below are point-to-point responses.

- Many pieces of essential work are missing, which should all appear in the main figures. I only list a few examples: the time series as classified by clusters, the diurnal variations of absorption for each cluster (to exclude the possible local sources), complete statistics of all parameters are required (BC mass, AAE, PM, compositions). Please do a complete and sound analysis and just show it. Otherwise, the conclusions are based on nowhere.

Response: We thank the reviewer for pointing out the shortcoming of our manuscript. Following the reviewer's suggestion, we have added a Fig. R1 below (also see Fig. 1 in the revised main text) to show the time series of light absorption (Abs(λ)) influenced by different clusters, a Fig. R2 below (also see Fig. S10 in the revised supporting information) to show the diurnal variations of Abs(λ) of each cluster, a Table R1 below (also see Table 1 in the revised manuscript) to summarize the optical parameters, and a Table R2 below (also see Table 2 in the revised main text) to summarize the mass concentrations of $PM_{2.5}$ and chemical species.

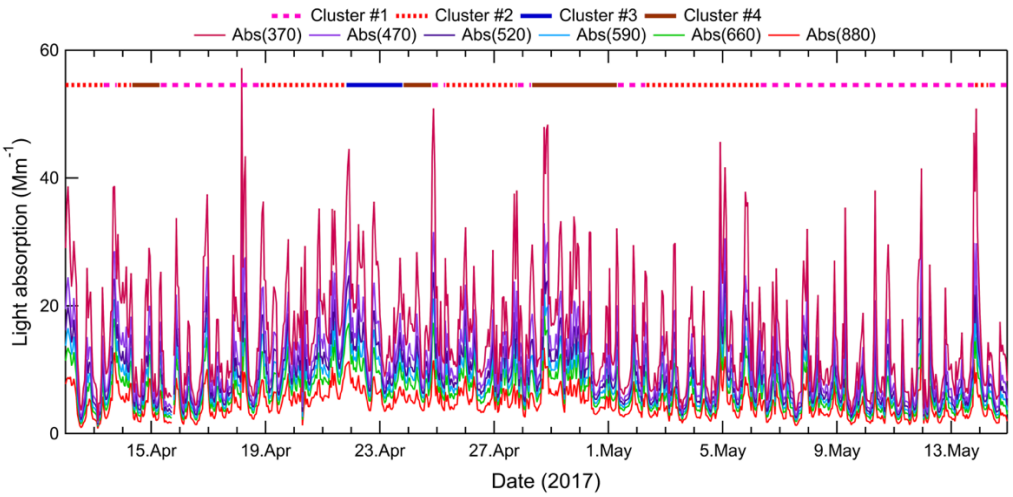

Figure R1. Time series of hourly averaged light absorption at different wavelengths (Abs(λ), λ = 370, 470, 520, 590, 660, and 880 nm). The different types of horizontal lines represent the four clusters of air masses.

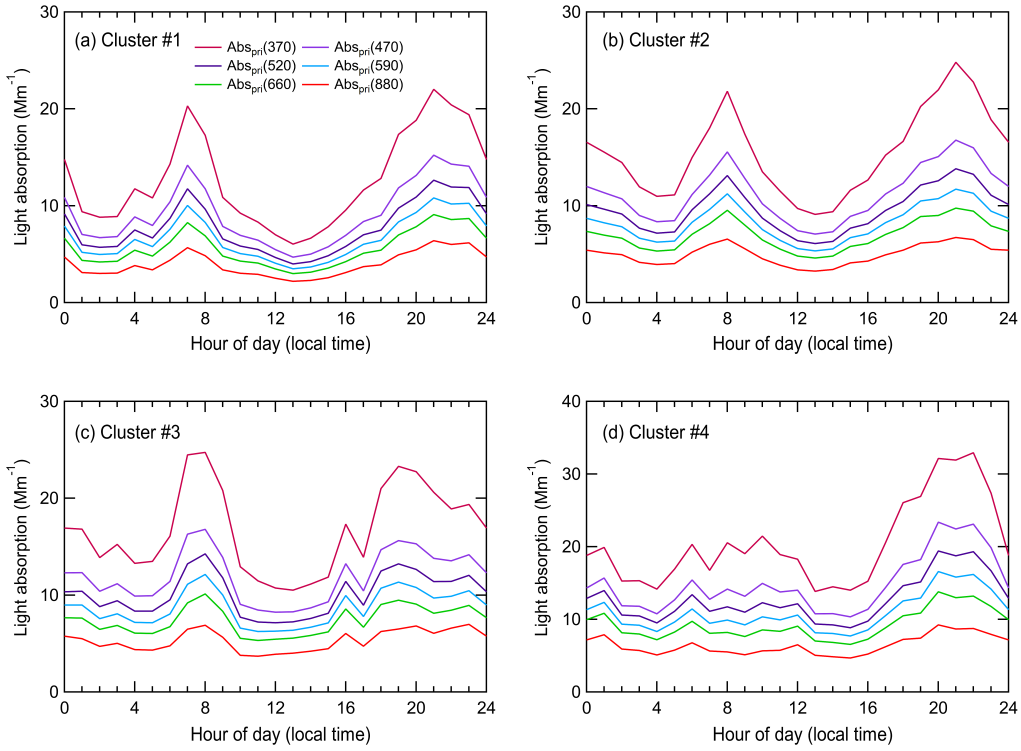

Figure R2. Diurnal variations of light absorption from primary emissions ($Abs_{pri}(\lambda)$, λ = 370, 470, 520, 590, 660, and 880 nm) in different clusters.

Table R1. Summary of light absorption at different wavelengths (Abs(λ), λ = 370, 470, 520, 590, 660, and 880 nm) and absorption Ångström exponent (AAE) of different emission sources.

Parametera	Average	Standard deviation
Abs(370) (Mm^{-1})	15.7	5.3
Abs(470) (Mm^{-1})	11.4	3.7
Abs(520) (Mm^{-1})	9.7	3.0
Abs(590) (Mm^{-1})	8.3	2.6
Abs(660) (Mm^{-1})	7.0	2.2
Abs(880) (Mm^{-1})	4.9	1.5
AAEtotal	1.41	0.05
AAEship	1.06	0.03
AAEbiomass	1.75	0.06
AAEvehicle	0.96	0.06

[a]AAE_{total} represents the AAE caused by total light-absorbing aerosols while AAE_{ship}, $AAE_{biomass}$, and $AAE_{vehicle}$ are AAE from ship emissions, biomass burning, and motor vehicle emissions, respectively.

Table R2. The average mass concentrations of carbonaceous matter, water-soluble ions, inorganic elements, and organics during the campaign.

Types	Species	Average	Standard deviation
$PM_{2.5}$ ($\mu g\ m^{-3}$)		14.3	4.2
Carbonaceous matter ($\mu g\ m^{-3}$)	organic carbon	2.7	1.1
	elemental carbon	0.8	0.3
Water-soluble ions ($\mu g\ m^{-3}$)	Na^+	0.5	0.2
	NH_4^+	0.6	0.4
	K^+	0.2	0.1
	Mg^{2+}	0.05	0.02
	Ca^{2+}	0.2	0.1
	Cl^-	0.23	0.2
	NO_3^-	0.6	0.3
	SO_4^{2-}	3.5	1.2
Inorganic elements ($ng\ m^{-3}$)	Ti	13.1	9.7
	V	2.4	1.4
	Mn	5.1	2.7
	Fe	127.3	78.9
	Ni	1.1	0.6
	Cu	28.0	14.4
	Zn	16.6	11.1
	Br	2.6	2.0
Organics ($ng\ m^{-3}$)	hopanes	0.2	0.05

- many issues here regarding the source attribution. The local source influence needs to be clearly excluded, or by some way to show it is of minor influence compared to the regional sources you stated.

Response: We thank the reviewer pointing out the influence of local emissions. Our sampling site is not located at a background area, therefore the influence of local emissions cannot be neglected. As a coastal city near the South China Sea, one of our objectives is to emphasize the ship emissions transported from ocean. Given that the air masses from the South China Sea are unable to carry pollutants from biomass burning, motor vehicles, and fugitive dust, these sources were possibly mainly

influenced by local emissions. In the revised manuscript, we used diurnal patter and concentration-weighted trajectory (CWT) analysis to indicate the influences of local emissions and regional transport. We have reworked the relevant discussion to make it more clearly, and it now reads as follows:

"To identify the possible source areas that affected $Abs_{pri}(\lambda)$, CWT analysis was performed based on the three-day backward trajectories. Large CWT values were mainly concentrated in the South China Sea (Fig. S9), highlighting the effect of ship emissions on aerosol light absorption. Additionally, the three-day backward trajectories were grouped into four cluster-mean trajectories to investigate the impact of different sources on $Abs_{pri}(\lambda)$ (Fig. 4). The air masses associated with Cluster #1 originated from the South China Sea. The $Abs_{ship}(\lambda)$ was the largest contributor in this cluster constituting 44–45% of $Abs_{pri}(\lambda)$ due to the high vessel traffic density over the South China Sea, consistent with the CWT results. Cluster #1 accounted for about 44% of the total trajectories, suggesting that Sanya was subjected to the influence of ship exhaust-related LAC aerosols, transported from the South China Sea. It is noteworthy that the diurnal pattern of $Abs_{pri}(\lambda)$ showed typically high values in the mornings and evenings (Fig. S10). This was attributed to the daily anthropogenic activities and variations in height of the planetary boundary layer. Given that the air masses from the South China Sea are unable to carry pollutants from biomass burning, motor vehicles, and fugitive dust, these sources were possibly mainly influenced by local emissions.

Cluster #2 originated from the South China Sea near the Indochina Peninsula and accounted for 35% of the total trajectories. The $Abs_{ship}(\lambda)$ was also vital in this cluster, accounting for 34–37% of $Abs_{pri}(\lambda)$. Fig. S10 shows that the $Abs_{pri}(\lambda)$ of Cluster #2 displayed a similar diurnal trend as that of Cluster #1. Considering that the air masses of Cluster #2 also originated from the South China Sea, the sources except for ship emissions were mainly influenced by local discharge. A small number of air masses were grouped into Cluster #3 and Cluster #4, accounting for only 6% and 15% of total trajectories, respectively. Cluster #3

originated from southern Burma and passed over Thailand, Laos, and Vietnam. On the other hand, Cluster #4 had the longest cluster-mean trajectory which originated and passed through the coastal areas of South-eastern China. Biomass burning was the dominant contributor to $Abs_{pri}(\lambda)$ in both clusters, with 62–69% for Cluster #3 and 56–64% for Cluster #4. Moreover, the $Abs_{biomass}(\lambda)$ of Cluster #3 and Cluster #4 were 1.8–4.4 times higher than those of Cluster #1 and Cluster #2. Since the $Abs_{biomass}(\lambda)$ from Cluster #1 and Cluster #2 were mainly attributed to local emissions, the higher values in Cluster #3 and Cluster #4 may have been influenced by the long-range transport of biomass burning from Southeast Asia and South-eastern China, where there was a large number of fire incidences (Fig. 4)."

Not clear with the definition of secondary substance, most organic and mineral should also be primary?

Response: The organics contains primary emissions and secondary formation, and the mineral dust here is fugitive dust. In our study, we used the BC-tracer method with MRS approach to distinguish the light absorption contributed by primary emissions (including black carbon and primary brown carbon) and secondary formation (that is secondary brown carbon). As the results shown in the main text, ~95% of light absorption was contributed by primary emissions. The reason why we wanted to prove this was that there was lack of tracers of secondary brown carbon when we did the PMF model. The negligible impact of secondary formation on light absorption can avoid potential uncertainty of not obtaining the secondary brown carbon in the optical source apportionment. However, the minor light absorption of secondary BrC did not mean that the mass concentration of secondary organic aerosol was low. It only indicated that few secondary organic aerosols had the light-absorbing ability. To eliminate the misunderstanding on this aspect, we revised our original expressions to "Based on Eq. (5), $Abs_{sec}(\lambda)$ accounted for less than 5% of $Abs(\lambda)$ (Table S1), suggesting a negligible impact of secondary formation on the light absorption capacity of aerosols during the study. Therefore, the uncertainty caused by using only $Abs_{pri}(\lambda)$ in the model could be

put to rest in the absence of an effective way to identify the source of secondary BrC."

Where did the dust come from, I don't think there was any dust sources rather than some sea salt.

Response: We agree with the reviewer that the sea salt is an important component in particulate matter at coastal city. However, the sea salt is a scattering material which is beyond the scope of our study. Here the dust denotes the fugitive dust which was mainly caused by the winds or relevant human activities in Sanya. In order to make it more clearly, we have changed the 'mineral dust' to 'fugitive dust' in the revised manuscript.

The shipping emissions are not really supported with any other external data source (I don't know what is that because I can't see anything from the current analysis done so far).

Response: We agree with the reviewer that more external tracers of ship emissions can further strengthen the identification results. However, the tracers were hard to determine due to the lack of effective chemical analysis method in this study. Actually, the V is a reliable tracer to indicate the ship emissions used in previous studies (e.g., Tao et al., 2016; Mamoudou et al., 2018). The V/Ni ratio can be further used to identify the ship emissions because it varies from 2.5 to 4.0 for this source (Cesari et al., 2014). In the case of lack of other external tracers, the current used V-based identification method in PMF model is also a reliable approach. To strengthen the reliability of our results, we have added more description about the verification of the PMF in the revised manuscript (see next response below).

References:

Cesari, D., Genga, A., Ielpo, P., Siciliano, M., Mascolo, G., Grasso, F. M., and Contini, D.: Source apportionment of $PM_{2.5}$ in the harbour–industrial area of Brindisi (Italy): Identification and estimation of the contribution of in-port ship emissions, Sci. Total Environ., 497–498, 392–400, https://doi.org/10.1016/j.scitotenv.2014.08.007, 2014.

Mamoudou, I., Zhang, F., Chen, Q., Wang, P. and Chen, Y.: Characteristics of PM2.5

from ship emissions and their impacts on the ambient air: A case study in Yangshan Harbor, Shanghai, Sci. Total Environ., 640–641, 207–216, https://doi.org/10.1016/j.scitotenv.2018.05.261, 2018.

Tao, J., Zhang, L., Cao, J., Zhong, L., Chen, D., Yang, Y., Chen, D., Chen, L., Zhang, Z., Wu, Y., Xia, Y., Ye, S. and Zhang, R.: Source apportionment of PM2.5 at urban and suburban areas of the Pearl River Delta region, south China - With emphasis on ship emissions, Sci. Total Environ., 574, 1559–1570, https://doi.org/10.1016/j.scitotenv.2016.08.175, 2017.

- The PMF analysis seems not quite convincing, could you provide more details about the scenarios.

Response: Following the reviewer's suggestion, we have added more descriptions about the verification of the PMF results (e.g., BS, DISP, and BS-DISP analysis) in the revised manuscript. It now reads as follows:

"Moreover, two to seven factors were selected to initiate the PMF5.0 run. Due to the additional factors, the Q/Q_{exp} ratio decreased with the increased number of factors as shown in Fig. S7. The decrease in Q/Q_{exp} was large when the factor number changed from 2 to 3 and 3 to 4 but stabilized as the factor number grew larger than 4, indicating that four factors may be the optimal solution. After multiple runs of the PMF5.0 model, four factor sources including ship emissions, motor vehicle emissions, biomass burning, and fugitive dust were finally identified (Fig. 3a). Additionally, the modeled $Abs_{pri}(\lambda)$ at different wavelengths showed strong correlations with the measured $Abs(\lambda)$ ($r = 0.82–0.89$, $p < 0.01$, Fig. S8). The slopes of 0.92–0.98 were consistent with the absorption fractions of $Abs_{pri}(\lambda)$ estimated by the BC-tracer method combined with the MRS approach (Table S1). The scaled residuals for each species varied between -3 and +3.

The uncertainty of each factor profile was further evaluated using BS, DISP, and BS-DISP. The BS results showed that the reproducibility of each source factor

was larger than 80% (Table S2), indicating good stability. Therefore, this suggested that the four source factors were appropriate. No swaps occurred in DISP, indicating the stability of the selected solution. Furthermore, all BS-DISP runs were successful. Overall, these results pointed to the efficiency of the PMF5.0 model in performing optical source apportionment."

And even so, would you really believe to incorporate the spectral absorption in parallel with the offline composition will really give some physical meaning? There seems no signature of sources on the absorption.

Response: We agree with the reviewer that there is no special signature of sources for one single-wavelength light absorption. However, when we use multiwavelength light absorption data together (e.g., λ = 370, 470, 520, 590, 660, and 880 nm in this study), there will be certain indication for specific sources due to the different light-absorbing aerosols having distinct absorption properties. For example, brown carbon, which is mainly from biomass burning, absorbs light towards short wavelengths (e.g., near-ultraviolet region). Therefore, compared to the fossil fuel sources, the biomass burning can contribute more to light absorption in the near-ultraviolet region (e.g., λ = 370 nm). Moreover, this contribution decreases with increase in wavelength. In contrast, the motor vehicle emissions contribute less to light absorption at λ = 370 nm than biomass burning due to the presence of large amounts of black carbon. This contribution increases with increase in wavelength. From this perspective, the additional multiwavelength absorption data in the PMF model will be helpful for optimizing the performance of source apportionment.

The time resolution is different between online and offline measurements, did you just average the online data into a very low time interval.

Response: Yes, we averaged the period of online data to match each filter sampling time. In the revised manuscript, we have added a sentence to clarify this:

"Online $Abs_{pri}(\lambda)$ data was integrated to match each filter sampling time."

- MAC of organic should be normalized by organic matter (including all elements) not only organic carbon. The MAC of organic here doesn't mean anything.

Response: We followed the reviewer's suggestion and changed to discuss the MAC of organic matter instead of organic carbon. The relevant content in the main text and figure (Fig. 6 in the revised manuscript) were revised accordingly. The update calculation method in the revised manuscript is shown as follows:

"Additionally, MAC could be used to reflect the light absorption capacity of aerosols. The MACs of BC and BrC at different wavelengths ($MAC_{BC}(\lambda)$ and $MAC_{BrC}(\lambda)$, respectively) were calculated with $Abs_{BC}(\lambda)$ and $Abs_{BrC}(\lambda)$ divided by the corresponding mass concentrations of BC and organic matter (OM), respectively:

$$MAC_{BC}(\lambda) = \frac{Abs_{BC}(\lambda)}{[BC]} \quad (7)$$

$$MAC_{BrC}(\lambda) = \frac{Abs_{BrC}(\lambda)}{[OM]} \quad (8)$$

where the mass concentration of OM was estimated by a factor of 1.8 times that of OC mass concentration (Turpin and Lim, 2001)."

- I am not convinced with the forcing calculation and the directly correlated heating. I don't think you really need to make that calculation as the main job of this study is to get the absorption attribution properly. The forcing largely replies on the vertical distribution of AOD and SSA, which you don't really have such information, which is beyond the scope of this study though.

Response: We thank the reviewer pointing out this. The direct radiative effect (DRE) caused by light-absorbing carbonaceous (LAC) aerosols is mainly related to their light absorption properties. So, it will be valuable for further estimating the source-specific LAC DRE after we obtained the light absorption of different sources. We agree with the reviewer that aerosol DRE strongly relies on the vertical distributions of AOD and SSA. The Optical Properties of Aerosols and Clouds (OPAC) model is a mature and widespread approach used in current studies to retrieve the vertical AOD and SSA based

on the surface measurements of chemical composition (e.g., Singh et al., 2018; Zhao et al., 2019; Kant et al., 2020). In our study, we used the OPAC model combining the measured mass concentrations of OC, EC, and water-soluble ions as well as the estimated mineral dust to estimate the vertical AOD, SSA, and AP. These optical parameters are essential inputs in the SBDART model for calculation of aerosol DRE. After careful consideration, we think that the reviewer's puzzle may be caused by our original unclear description in models of OPAC and SBDART. Therefore, we added more information about the calculations of OPAC (e.g., compared with the PAX measured light extinction and the satellite-derived AODs) and SBDART model in the revised manuscript. It now reads as follows:

"**2.7 The Optical Properties of Aerosols and Clouds (OPAC) Model**

The OPAC model was used to retrieve the following parameters: aerosol optical depth (AOD), single scattering albedo (SSA), and asymmetric parameter (AP). The parameters were important in estimating the radiative effect of aerosols. A detailed description of the OPAC software package was given by Hess et al. (1998). The measured mass concentrations of OC, EC, and water-soluble ions as well as the estimated mineral dust loading (=[Fe]/0.035) during the day were used in the OPAC model to estimate the optical parameters. Moreover, the BC number concentration in the OPAC model was constrained by the measured BC mass concentration. Although several water-soluble ions and mineral dust were obtained, they did not contain all the water-soluble and insoluble material. Therefore, based on the measured data, the number concentrations of water-soluble and insoluble materials were tuned. This was done until the differences between the OPAC-derived light scattering, light absorption, and SSA versus the corresponding PAX-measured values were within 5% (Fig. S3). After the aerosol light extinction coefficient (sum of light scattering and absorption) was obtained, the AOD was estimated as follows (Hess et al., 1998):

$$\mathrm{AOD} = \sum_j \int_{H_{j,min}}^{H_{j,max}} \sigma_{e,j}(h)dh = \sum_j \sigma_{e,j}^1 N_j(0) \int_{H_{j,min}}^{H_{j,max}} e^{-\frac{h}{Z_j}} dh \quad (12)$$

where $H_{j,max}$ and $H_{j,min}$ were the upper and lower boundaries in layer j; $\sigma_{e,j}$

was the surface aerosol light extinction coefficient in layer j; h was the layer height; $\sigma_{e,j}^{1}$ represented the aerosol light extinction coefficient that was normalized to 1 particle cm^{-3}; N_j was the number concentration in layer j; and Z was the scale height. Furthermore, the OPAC-derived AODs were tuned to match the satellite-derived AODs (https://giovanni.gsfc.nasa.gov/giovanni, last access: January 2020) by altering the scale height in OPAC until the difference between them was within 5%. Owing to closure with AOD and anchoring of chemical composition, the assumptions in the OPAC model did not have a significant impact on the estimation of radiative effect in subsequent section 2.8 (Satheesh and Srinivasan 2006).

2.8 Estimations of radiative effect and heating rate

The LAC direct radiative effect (DRE) was estimated by the Santa Barbara DISORT (Discrete Ordinate Radiative Transfer) Atmospheric Radiative Transfer (SBDART) model in the shortwave spectral region of 0.25–4.0 μm. A detailed description of the SBDART model was given by Ricchiazzi et al. (1998). The AOD, SSA, and AP are essential input parameters in the SBDART model and were obtained from the OPAC model (see section 2.7). In addition to these, several other input parameters were included, namely the surface albedo, solar zenith angle, and profiles of atmospheric parameters. The surface albedo was derived from the Moderate Resolution Imaging Spectroradiometer (https://modis-atmos.gsfc.nasa.gov/ALBEDO/index.html, last access: January 2020). On the other hand, the solar zenith angle was calculated with a specific time and location (i.e., latitude and longitude) using a small code from the SBDART model. Furthermore, six standard atmospheric vertical profiles (i.e., tropical, mid-latitude summer, subarctic summer, mid-latitude winter, subarctic winter and US62) were embedded in the SBDART model. They provided vertical distributions of temperature, pressure, water vapor, and ozone density (Ricchiazzi et al., 1998). In this study, the mid-latitude summer was selected to represent the situation of Sanya based on its classification as a mid-latitude

region. Obregón et al. (2015) demonstrated that the SBDART model could provide a reliable estimation of radiative effect. Moreover, aerosol DRE was defined as the difference in the radiation flux (F) either at the Earth's surface or at the top of the atmosphere, respectively with and without the aerosol in the atmosphere:

$$DRE = (F\downarrow - F\uparrow)_{\text{with aerosol}} - (F\downarrow - F\uparrow)_{\text{without aerosol}} \quad (13)$$

where $\downarrow$ and $\uparrow$ represented the downward and upward flux, respectively. Atmospheric DRE was then estimated by the difference between the DRE at the top of the atmosphere and the Earth's surface.

Further, the atmospheric heating rate ($\frac{\partial T}{\partial t}$, in unit of K d^{-1}) caused by LAC aerosols was estimated using the first law of thermodynamics and hydrostatic equilibrium as follows (Liou, 2002):

$$\frac{\partial T}{\partial t} = \frac{g}{C_p} \times \frac{\Delta F}{\Delta P} \quad (14)$$

where $\frac{g}{C_p}$ was the lapse rate and g stood for acceleration due to gravity while C_p described the specific heat capacity of air at a constant pressure (1006 J kg^{-1} K^{-1}). Additionally, ΔF was the atmospheric DRE contributed by LAC aerosols and ΔP represented the atmospheric pressure difference (300 hPa)."

References:

Kant, Y., Shaik, D. S., Mitra, D., Chandola, H. C., Babu, S. S. and Chauhan, P.: Black carbon aerosol quantification over north-west Himalayas: Seasonal heterogeneity, source apportionment and radiative forcing, Environ. Pollut., 257, 113446, https://doi.org/10.1016/j.envpol.2019.113446, 2020.

Singh, S., Tiwari, S., Hopke, P. K., Zhou, C., Turner, J. R., Panicker, A. S. and Singh, P. K.: Ambient black carbon particulate matter in the coal region of Dhanbad, India, Sci. Total Environ., 615, 955–963, https://doi.org/10.1016/j.scitotenv.2017.09.307, 2018.

Zhao, S., Yu, Y., Yin, D., Yu, Z., Dong, L., Mao, Z., He, J., Yang, J., Li, P. and Qin, D.: Concentrations, optical and radiative properties of carbonaceous aerosols over

urban Lanzhou, a typical valley city: Results from in-situ observations and numerical model, Atmos. Environ., 213, 470–484, https://doi.org/10.1016/j.atmosenv.2019.06.046, 2019.

- No need such redundant description for the trajectory clustering, as this is not your original work and has been so widely used previously, which was just output using some user-friendly software.

Response: Following the reviewer's suggestion, we briefly described the method of trajectory cluster analysis in the revised manuscript. It now reads as follows:

"Cluster analysis of three-day backward air-mass trajectories was used to investigate the impact of transport pathways on Abs(λ). The backward trajectories were calculated hourly with an arrival height of 500 m above ground level using the Hybrid Single-Particle Lagrangian Integrated Trajectory Model (Draxler and Rolph, 2003). The cluster analysis was performed according to the angle-based distance statistics method (Q. Wang et al., 2018a). Furthermore, a Concentration-weighted Trajectory (CWT) analysis based on the three-day backward trajectories was used to identify the potential source areas (Q. Wang et al., 2016). Finally, cluster and CWT analyses were performed using a GIS-based TrajStat software developed by Wang et al. (2009)."

Optical source apportionment and radiative effect of light-absorbing carbonaceous aerosols in a tropical marine monsoon climate zone: The importance of ship emissions

Qiyuan Wang[1,2], Huikun Liu[1], Ping Wang[3], Wenting Dai[1], Ting Zhang[1], Youzhi Zhao[3], Jie Tian[1], Wenyan Zhang[1], Yongming Han[1,2], Junji Cao[1,2]

[1]Key Laboratory of Aerosol Chemistry and Physics, State Key Laboratory of Loess and Quaternary Geology, Institute of Earth Environment, Chinese Academy of Sciences, Xi'an 710061, China
[2]CAS Center for Excellence in Quaternary Science and Global Change, Xi'an 710061, China
[3]Hainan Tropical Ocean University, Sanya 572022, China

Correspondence to: Qiyuan Wang (wangqy@ieecas.cn) and Junji Cao (cao@loess.llqg.ac.cn)

Abstract. Source-specific optical properties of light-absorbing carbonaceous (LAC) aerosols in the atmosphere are poorly understood because they are generated by various sources. In this study, a receptor model combining multi-wavelength absorption and chemical species was used to explore the source-specific optical properties of LAC aerosols in a tropical marine monsoon climate zone. The results showed that biomass burning had the largest contribution to average LAC absorption. However, ship emissions emerged as the dominant contributors (44–45%) when the air masses originated from the South China Sea. Additionally, the source-specific Absorption Ångström Exponent (AAE) indicated that black carbon (BC) was the dominant LAC aerosol in ship and motor vehicle emissions. Moreover, brown carbon (BrC) was present in biomass-burning emissions. The source-specific mass absorption cross section (MAC) showed that BC from ship emissions had a stronger light-absorbing capacity compared to emissions from biomass burning and motor vehicles. The BrC MAC derived from biomass burning was also smaller than the BC MAC and was highly depended on wavelength. Furthermore, radiative effect assessment indicated a comparable atmospheric forcing and heating capacity of LAC aerosols between biomass burning and ship emissions. This study provides insights into the optical properties of LAC aerosols from various sources. It also sheds more light on the radiative effects of LAC aerosols generated by ship emissions.

删除了: **forcing**
删除了: **at**
删除了: **t**
删除了: owing to its
删除了: in the atmosphere
删除了: Here
删除了: coupling
删除了: with
删除了: utilized
删除了: LAC
删除了: at
删除了: R
删除了: contributed
删除了: on average
删除了: , but
删除了: became
删除了:
删除了:
删除了: T
删除了: a
删除了: e
删除了: s
删除了: while there was also
删除了: existed
删除了: than
删除了: emissions
删除了: s
删除了: R
删除了: s
删除了: from
删除了: Our
删除了: and can improve our understanding of
删除了: LAC
删除了: caused

1 Introduction

Carbonaceous aerosols are abundant in $PM_{2.5}$ (particulate matter with an aerodynamic diameter ≤ 2.5 μm) (e.g., 20–50% of $PM_{2.5}$ mass, Putaud et al., 2010; Tao et al., 2017) and have extensively been explored due to their implications on global climate forcing (IPCC, 2013). Among the complex carbonaceous compounds are the light-absorbing carbonaceous (LAC) aerosols which are mainly associated with absorption of light. LAC aerosols consist of black carbon (BC) and brown carbon (BrC). BC is a short-lived climate forcer with a strong ability to absorb sunlight. Moreover, it is regarded as the second largest contributor of positive anthropogenic climate forcing after carbon dioxide (Bond et al., 2013). On the other hand, BrC refers to a class of light-absorbing organic compounds with enhanced light absorption at short wavelengths (e.g., near-ultraviolet region). Therefore, it is a potential contributor to atmospheric heating at both global and regional scales (Laskin et al., 2015).

The optical properties of LAC aerosols are closely related to their sources as well as atmospheric conditions and secondary processing. However, distinguishing source-specific light absorption by LAC from a mixture of aerosols in the atmosphere is still a challenge. It is possible to use multi-wavelength light absorption data to identify optical source apportionment based on the Beer-Lambert's Law (e.g., aethalometer model and multi-wavelength absorption analyzer model, Sandradewi et al., 2008; Massabò et al., 2015), which can typically explain two different types of sources (e.g., fossil fuels versus biomass burning). Results from this method are highly dependent on the use of the source-specific Absorption Ångström Exponent (AAE). However, due to lack of source-specific AAE data, most studies use empirical values reported in previous literature (e.g., Healy et al., 2017; Küpper et al., 2018; Zheng et al., 2019). This may create inconsistencies in the reported results because the source-specific AAEs varies with the type of fuels and their burning efficiencies (Tian et al., 2019).

In addition, optical source apportionment can be obtained using receptor models (e.g., Positive Matrix Factorization (PMF) and Multilinear Engine (ME2)). Several studies have utilized receptor models to identify sources, first based on the sole chemical species or mass spectra information. Thereafter, a multiple linear regression model is used to apportion the contribution of each source to the optical parameters of an aerosol (Qin et al., 2018; Tian et al., 2020). This method may be referred to as indirect optical source apportionment. In contrast, Forello et al. (2019) coupled chemical species with multi-

删除了: is…ubiquitous in the atmosphere and is …bundant in $PM_{2.5}$ (particulate matter with an aerodynamic diameter ≤ 2.5 μm) (e.g., 20 … …0% of $PM_{2.5}$ mass) (… Putaud et al., 2010; Tao et al., 2017) and. It has been…have extensively been explored concerned …ue to its …heirsignificant…implications for …n global climate forcing (IPCC, 2013). Among the complex carbonaceous composition…ompounds are, there is a group of substances in relation with…the light absorption, which is named…light-absorbing carbonaceous (LAC) aerosols which are mainly associated with absorption of light. The …AC aerosols consists…of black carbon (BC) and brown carbon (BrC). BC is a short-lived climate forcer with a strong ability to absorb sunlight. Moreover, it is absorption and has been…regarded as the second largest contributor to …f positive anthropogenic positive …limate forcing after carbon dioxide (Bond et al., 2013). On the other hand, BrC refers to a class of light-absorbing organic compounds with enhanced light absorption at towards …hort wavelengths (e.g., near-ultraviolet region). and,…Tt…erefore, it is a potential contributor to atmospheric heating at both on ... [1]

删除了: LAC …ight absorption by LAC from a mixture of aerosols in the atmosphere is bulk one …till aremains…challengeing in the atmosphere… It is possibleOne can…to use multi-wavelength light absorption data to realize the…dentify optical source apportionment based on the Beer-Lambert's Law (e.g., aethalometer model and multi-wavelength absorption analyzer model,) (…Sandradewi et al., 2008; Massabò et al., 2015), which. This method…can typically explain two different types of sources (e.g., fossil fuels versus biomass burning). that contribute to LAC light absorption, and the r…Results from this method are highly dependent relied …n the use of the source-specific Aa…sorption Ångström Ee…ponent (AAE) used in models… However, owing …ue to the…lack of access to obtaining these…ource-specific AAE data, most studies applied …se empirical values reported in other …revious literatures…(e.g., Healy et al., 2017; Küpper et al., 2018; Zheng et al., 2019). This may create inconsistencies in the reportedlead to a large uncertainty to the…results,…because the source-specific AAEs are site-dependent variables and …aries with the type of fuels types ... [2]

删除了: also …e obtained usingrealized by…receptor models (e.g., Pp…sitive Mm…trix Ff…ctorization (PMF) and Mm…ltilinear Ee…gine (ME2)). Several studies have utilized a…receptor models to identify the …ources, firstly…based on the sole chemical species or mass spectra information. Thereafter,,…and then … multiple linear regression model is further …sed to apportion the contribution of each source to the aerosol…optical parameters of an aerosol (e.g., …in et al., 2018; Tian et al., 2020). This method can …ay be called … ... [3]

wavelength absorption in ME2 to directly perform optical source apportionment. Compared to the indirect approach, the additional optical data in receptor models can improve the performance of source apportionment because each source has its own optical features. Furthermore, it may eliminate potential uncertainties caused by multiple operations in the indirect approach. However, the application of direct optical source apportionment is scarce at the moment.

Alternatively, laboratory studies may effectively be used to explore the optical properties of LAC from a specific source (e.g., vehicle engine exhaust, coal combustion, and biomass burning) (Tian et al., 2019; Xie et al., 2017). However, the optical properties of LAC may significantly change due to the complex atmospheric processes that they undergo after emission into the atmosphere. Therefore, it is critical to identify LAC aerosols from different sources in the atmosphere using specific methods in order to obtain their optical properties. Furthermore, to the best of our knowledge, there is no study focusing on the optical properties of ship exhaust-related LAC aerosols in the atmosphere. This presents a challenge to our understanding of the role of ship emissions on the climate considering that it is a significant part of discharge from the transport sector.

In this study, multi-wavelength aerosol light absorption and chemical species were measured in Sanya, a coastal city in China. This was done to investigate the optical properties of LAC aerosols from ship emissions and other sources. A dataset combining optical and chemically speciated data was used simultaneously in a receptor model to obtain the optical source apportionment. Afterwards, the source-specific optical properties of LAC aerosols were determined and characterized. Finally, the impact of radiative effect induced by LAC aerosols from different sources was evaluated. This study provides insights into the source-specific optical properties of LAC aerosols from various sources. Additionally, it reinforces knowledge on the radiative effects of LAC aerosol.

2 Methodology

2.1 Sampling site

The sampling site is located in Sanya, a small city (an area of 1921.5 km^2 and a total population of 0.59 million as at 2017) in the southernmost tip of the Hainan Island in Southern China (Fig. S1).

删除了: the …ptical source apportionment. Compared with …o the indirect approach, the additional optical data in receptor models can improve the performance of source apportionment,…because each source has its own optical features. Furthermore, it may eliminatealso avoid some…potential uncertainties caused by multiple operations of …n the indirect approach. However, the application of direct optical source apportionment is scarce lack …t the momentpresent ... [4]

删除了: y is also an…effectively be used way…to explore the characteristics of LAC …ptical properties of LAC from a specific source (e.g., vehicle engine exhaust, coal combustion, and biomass burning) (Tian et al., 2019; Xie et al., 2017). However, owing to the complex atmospheric processes experienced by LAC aerosol after it emitted to the atmosphere, …he features of LAC…optical properties LAC may change …ignificantly change due to the complex atmospheric processes that they undergo after emission into the atmosphere. Thereforeus… it is critical to identify the…LAC aerosols fromof…different sources in the atmosphere through …sing specific certain …ethods in order to obtain their optical properties. Furthermore, as an important part of emissions from transportation sector, …o the best of our knowledge, there is no study focusing on the optical properties of ship exhaust-related LAC aerosols in the atmosphere. This presents a challenge to hinders …ur in-depth …nderstanding of the role of ship emissions on thein…climate considering that it is a significant part of discharge from the transport sector effects ... [5]

删除了: of…China. This was done to investigate the LAC …ptical properties of LAC aerosols from ship emissions and other sources. The … dataset joining …ombining optical and chemically speciated data was used simultaneously in a receptor model to realize …btain the optical source apportionment. Afterwards; then… the source-specific LAC …ptical properties of LAC aerosols were determined and characterized.;…Ff…nally, the impacts…of radiative forcing …ffect induced by LAC aerosols from different sources were …as evaluated. Our …his study provides insights into the source-specific LAC …ptical properties of LAC aerosols from various sources. Additionally, it reinforces knowledge onand will improve our understanding of ... [6]

删除了: in…2017) inat…the southernmost tip of the Hainan Island in Ss… ... [7]

Comprehensive measurements were taken in spring from 12th April to 14th May 2017 on the rooftop of a teaching building (about 20 m above ground level) in Hainan Tropical Ocean University (18.30° N, 109.52° E). The sampling site is predominantly an educational and residential area with typical urban sources of emission including vehicles and cooking appliances. Sanya lies within a tropical marine monsoon climate zone therefore the weather was warm (temperature = 28 ± 3°C) and wet (relative humidity = 81 ± 12%) during the study.

2.2 Online and offline measurements

A model AE33 aethalometer (Magee Scientific, Berkeley, CA, USA) was used to determine the light absorption coefficients of the aerosols at multi-wavelengths (Abs(λ), λ is wavelength) with a $PM_{2.5}$ cyclone (SCC 1.829, BGI Inc. USA). Briefly, the collected particles were desiccated using a Nafion® dryer (MD-700-24S-3; Perma Pure, Inc., Lakewood, NJ, USA) before measurement with the AE33 aethalometer. As shown in Fig. S2, the loss of Abs(λ) caused by the dryer was ignored. Afterwards, seven light emitting diodes (λ = 370, 470, 520, 590, 660, 880, and 950 nm) in the AE33 aethalometer were used to irradiate the filter deposition spot to obtain light attenuation as previously described (Drinovec et al., 2015). Since the AE33 aethalometer records the BC mass concentrations, the Abs(λ) at each wavelength were retrieved by getting the product of BC mass concentration ([BC]) and mass absorption cross-section (MAC) used in the instrument (Abs(λ) = [BC] × MAC) (Drinovec et al., 2015). One of the advantages of AE33 aethalometer is that it resolves the filter loading effect using a dual-spot compensation technique. Further details regarding the principles of operation of the AE33 aethalometer have been outlined by Drinovec et al. (2015).

In addition, A Photoacoustic Extinctiometer (PAX, Droplet Measurement Technologies, Boulder, CO, USA) was used to directly measure aerosol light absorption at λ = 532 nm. It was set in parallel with the AE33 aethalometer using the same $PM_{2.5}$ cyclone and Nafion® dryer. Briefly, the PAX adopts an intracavity photoacoustic technique, with a modulated laser beam heating up the sampled particles in an acoustic chamber. The pressure wave generated from heating is then detected by a sensitive microphone. Moreover, aerosol light scattering can be measured using a wide-angle integrating reciprocal nephelometer in a scattering chamber. In this study, different concentration gradients of ammonium

删除了: Intensive
删除了: conducted
设置了格式: 上标
删除了: at
设置了格式: 上标
删除了: at
删除了: surrounded by
删除了: no obvious pollution
删除了: in the vicinity
删除了: As
删除了: ,
删除了: of Sanya
删除了: campaign
删除了: M
删除了: aerosol
删除了: T
删除了: with
删除了: they measured by
删除了: described previously
删除了: are
删除了: the
删除了: measurement
删除了: More
删除了: AE33
删除了: can be found in
删除了: p
删除了: e
删除了: the
删除了: T
删除了: os
删除了: heating generated
删除了: Meanwhile
删除了: the
删除了: also
删除了: with
删除了: During the campaign,

sulphate and freshly-generated propane soot were used to calibrate light scattering and absorption measurements, respectively. The calibration procedure was described in detail by Q. Wang et al. (2018a). The $PM_{2.5}$ quartz-fiber filters (8 × 10 inch) (QM/A; GE Healthcare, Chicago, IL, USA) were collected during the day (from 08:00 to 20:00) and at night (from 20:00 to 08:00 the next day) using a high-volume air sampler (Tisch Environmental, Inc., USA) with a flowrate of 1.13 m^3 min^{-1}. Before sampling, the blank quartz-fiber filters were heated in a muffle furnace at 805 °C for 3h to remove possible impurities. After sampling, the quartz-fiber filters were saved in a freezer at about -20 °C to minimize evaporation of volatile materials before chemical analyses. Finally, field blanks were collected and analysed to eliminate potential background artifacts.

The collected quartz-fiber filters were used to analyse inorganic elements, carbonaceous matter, water-soluble ions, and organics. An Energy-Dispersive X-ray Fluorescence (ED-XRF) spectrometry (Epsilon 5 ED-XRF, PANalytical B.V., Netherlands) was used to determine the Titanium (Ti), Vanadium (V), Manganese (Mn), Ferrum (Fe), Nickel (Ni), Copper (Cu), Zinc (Zn), and Bromine (Br) quantities. A detailed description of the principles of ED-XRF has been highlighted by Xu et al. (2012). Moreover, a thermal/optical carbon analyzer (Desert Research Institute Model 2001, Atmoslytic Inc., Calabasa, CA, USA) was used to analyse organic carbon (OC) and elemental carbon (EC). A detailed analytical procedure has been described elsewhere (Chow et al., 2007). An Ion Chromatograph (IC, Dionex 600; Dionex Corporation, Sunnyvale, CA, USA) was also used to quantify the water-soluble cations (i.e., Na^+, K^+, Mg^{2+}, Ca^{2+}, and NH_4^+) and anions (i.e., Cl^-, NO_3^-, and SO_4^{2-}) as described by Zhang et al. (2011). Finally, an in-injection port Thermal Desorption (TD) coupled with an Agilent 7890/5975C Gas Chromatography/Mass Spectrometer (GC/MS) (Agilent Technologies, Santa Clara, CA, USA) was used to determine the hopanes using a protocol described by J. Wang et al. (2016).

2.3 Segregation of BC and BrC absorption

The Abs(λ) consisted of light absorption from both LAC aerosols (BC and BrC) and mineral dust (Wang et al., 2013). Therefore, LAC absorption ($Abs_{LAC}(\lambda)$) was calculated as follows:

$$Abs_{LAC}(\lambda) = Abs_{BC}(\lambda) + Abs_{BrC}(\lambda) = Abs(\lambda) - Abs_{mineral}(\lambda) \quad (1)$$

删除了：the…light scattering and absorption measurements, respectively. The calibration procedure is …as described in detail in ... [8]

删除了：time…(from 08:00 to 20:00) and at nighttime…(from 20:00 to 08:00 the next day) using a high-volume air sampler (Tisch Environmental, Inc., USA) with a flowrate of 1.13 m^3 min^{-1}. Before sampling, the blank quartz-fiber filters were heated in a muffle furnace at 805 °C for 3h to remove the…possible impurities. After sampling, the quartz-fiber filters were saved in a freezer at about -20 °C to minimize evaporation of volatile materials before chemical analyses. Finally, fF…eld blanks were collected and analysed to eliminate the ... [9]

删除了：e…ergy-Dd…spersive X-ray Ff…uorescence (ED-XRF) spectrometry (Epsilon 5 ED-XRF, PANalytical B.V., Netherlands) was used to determine the inorganic elements, including …t…tanium (Ti), Vv…nadium (V), Mm…nganese (Mn), Ff…rrum (Fe), Nn…ckel (Ni), Cc…pper (Cu), Zz…nc (Zn), and Bb…omine (Br) quantities. A detailed description of the principles of ED-XRF principle may…as been highlighted be found in…by Xu et al. (2012). Moreover, aA…thermal/optical carbon analyzer (Desert Research Institute Model 2001, Atmoslytic Inc., Calabasa, CA, USA) was used to analyse the carbonaceous matter, including …rganic carbon (OC) and elemental carbon (EC). More … detailed analytical procedure has been described elsewhere (Chow et al., 2007). An Ii…n Cc…romatograph (IC, Dionex 600; Dionex Corporation, Sunnyvale, CA, USA) was also used to quantify the water-soluble cations (i.e., Na^+, K^+, Mg^{2+}, Ca^{2+}, and NH_4^+) and anions (i.e., Cl^-, NO_3^-, and SO_4^{2-}). A detailed description of this instrument may be found…as described by in…Zhang et al. (2011). Finally, aA… in-injection port Tt…ermal Dd…sorption (TD) coupled with an Agilent 7890/5975C Gg…s Cc…romatography/Mm…ss Ss…ectrometer (GC/MS) (Agilent Technologies, Santa Clara, CA, USA) was used to determine the hopanes using a protocol described by. A detailed description of TD-GC/MS operation may be found in ... [10]

删除了：s…of light absorption from both caused by …AC aerosols (BC and BrC) and mineral dust (Wang et al., 2013). Therefore, The …AC absorption ($Abs_{LAC}(\lambda)$) therefore ... [11]

where $Abs_{BC}(\lambda)$, $Abs_{BrC}(\lambda)$, and $Abs_{mineral}(\lambda)$ were absorption of light by BC, BrC, and mineral dust at λ = 370, 470, 520, 590, 660, or 880 nm, respectively (in unit of Mm^{-1}). The $Abs_{mineral}(\lambda)$ was retrieved from the optical source apportionment as discussed in section 3.2. With an assumption of BC only absorbing at λ = 880 nm, the $Abs_{BC}(\lambda)$ at wavelengths of 370, 470, 520, 590, and 660 was extrapolated as follows:

$$Abs_{BC}(\lambda) = Abs(880) \times \left(\frac{\lambda}{880}\right)^{-AAE_{BC}} \quad (2)$$

where AAE_{BC} represents BC AAE, which was assumed to be 1.1 based on a study by Lack and Langridge (2013). Combining Eqs. (1) and (2) gave the following equation:

$$Abs_{BrC}(\lambda) = Abs(\lambda) - Abs(880) \times \left(\frac{\lambda}{880}\right)^{-AAE_{BC}} - Abs_{mineral}(\lambda) \quad (3)$$

From the perspective of emission and formation, the Abs(λ) could be divided into light absorption contributed by primary emissions ($Abs_{pri}(\lambda)$) and secondary formation ($Abs_{sec}(\lambda)$). Therefore, the Abs(λ) could be calculated as follows:

$$Abs(\lambda) = Abs_{pri}(\lambda) + Abs_{sec}(\lambda) \quad (4)$$

A BC-tracer method was utilized to separate $Abs_{sec}(\lambda)$ from $Abs_{pri}(\lambda)$ and the Eq. (4) could further be developed as follows (Wang et al., 2019a):

$$Abs_{sec}(\lambda) = Abs(\lambda) - \left(\frac{Abs(\lambda)}{BC}\right)_{pri} \times [BC] \quad (5)$$

where $\left(\frac{Abs(\lambda)}{BC}\right)_{pri}$ described the ratio of Abs(λ) to BC mass concentration in primary emissions (in unit of $m^2\ g^{-1}$), and [BC] denoted the mass concentration of BC in the atmosphere (in unit of $\mu g\ m^{-3}$). This was retrieved from the relationship between Abs(880) measured by the AE33 aethalometer and EC mass concentration. Finally, the $\left(\frac{Abs(\lambda)}{BC}\right)_{pri}$ ratio was determined using a minimum *R*-squared (MRS) method previously described by Wang et al. (2019a).

2.4 Estimation of optical parameters

AAE reflects spectral dependence of aerosol light absorption and can be used to distinguish the chemical composition of LAC aerosols. For example, LAC aerosol dominated by BC has an AAE close to 1.0 while the presence of BrC results in AAE larger than 1.0 (Andreae and Gelencsér, 2006). As described previously, AAE can be retrieved using a power law function as follows (Andreae and Gelencsér, 2006):

删除了: are
删除了: the light
删除了: contributed
删除了: below
删除了: only
删除了: can be
删除了: according to the
删除了: of
删除了: can
删除了: Thus
删除了: c
删除了: an
删除了: (Wang et al., 2019a)
删除了: . Thus,
删除了: can
删除了: be
删除了: s
删除了: ;
删除了: s
删除了: ,
删除了: which
删除了: T
删除了: with
删除了: , which is
删除了: in detail in
删除了: , which
删除了: as an indicator
删除了: ing

$$\mathrm{Abs}(\lambda) = \mathrm{C} \times \lambda^{-\mathrm{AAE}} \quad (6)$$

where C is a constant independent of wavelength.

Additionally, MAC could be used to reflect the light absorption capacity of aerosols. The MACs of BC and BrC at different wavelengths ($\mathrm{MAC_{BC}}(\lambda)$ and $\mathrm{MAC_{BrC}}(\lambda)$, respectively) were calculated with $\mathrm{Abs_{BC}}(\lambda)$ and $\mathrm{Abs_{BrC}}(\lambda)$ divided by the corresponding mass concentrations of BC and organic matter (OM), respectively:

$$\mathrm{MAC_{BC}}(\lambda) = \frac{\mathrm{Abs_{BC}}(\lambda)}{[\mathrm{BC}]} \quad (7)$$

$$\mathrm{MAC_{BrC}}(\lambda) = \frac{\mathrm{Abs_{BrC}}(\lambda)}{[\mathrm{OC}]} \quad (8)$$

where the mass concentration of OM was estimated by a factor of 1.8 times that of OC mass concentration (Turpin and Lim, 2001).

2.5 Receptor model source apportionment

The PMF version 5.0 (PMF5.0) from the US Environmental Protection Agency (Norris et al., 2014) was applied to determine the contribution of various sources to aerosol light absorption. The principle of PMF has been described elsewhere (Paatero and Tapper, 1994). Briefly, PMF decomposes the initial dataset into a factor contribution matrix $\mathrm{G_{ik}}$ ($i \times k$ dimensions) and a factor profile matrix $\mathrm{F_{kj}}$ ($k \times j$ dimensions) and then iteratively minimizes the object function Q:

$$\mathrm{X_{ij}} = \sum_{k=1}^{p} \mathrm{G_{ik}F_{kj}} + \mathrm{E_{ij}} \quad (9)$$

$$Q = \sum_{i=1}^{m} \sum_{j=1}^{n} \left(\frac{\mathrm{E_{ij}}}{\sigma_{ij}}\right)^2 \quad (10)$$

where $\mathrm{X_{ij}}$ was the value of the jth species in the ith sample; $\mathrm{E_{ij}}$ described the model residual; and σ_{ij} represented uncertainty, which was calculated as follows:

$$\sigma_{ij} = \begin{cases} \sqrt{(\text{error fraction} \times \text{concentration})^2 + (0.5 \times \mathrm{MDL})^2}, & (\text{concentration} > \mathrm{MDL}) \\ \frac{5}{6} \times \mathrm{MDL}, & (\text{concentration} \le \mathrm{MDL}) \end{cases} \quad (11)$$

where MDL was the method detection limit and the error fraction was set to 10% (Rai et al., 2020). The uncertainties of the PMF5.0 results were evaluated by the following analyses: Bootstrap (BS), Displacement (DISP), and Bootstrap-displacement (BS-DISP). The BS analysis assesses the random

删除了: The mass absorption cross-section (
删除了:) can
删除了: aerosol
删除了: ing
删除了: OC
删除了: Here t
删除了: s
删除了: Abs(λ)
删除了: ,
删除了: is
删除了: s
删除了: s
删除了: .

errors in PMF solutions while DISP estimates rotational ambiguity. On the other hand, BS-DISP estimates both random errors and rotational ambiguity. A more detailed description of the three error estimation methods has been provided by Paatero et al. (2014) and Brown et al. (2015).

2.6 Analysis of air-mass trajectories

Cluster analysis of three-day backward air-mass trajectories was used to investigate the impact of transport pathways on Abs(λ). The backward trajectories were calculated hourly with an arrival height of 500 m above ground level using the Hybrid Single-Particle Lagrangian Integrated Trajectory Model (Draxler and Rolph, 2003). The cluster analysis was performed according to the angle-based distance statistics method (Q. Wang et al., 2018a). Furthermore, a Concentration-weighted Trajectory (CWT) analysis based on the three-day backward trajectories was used to identify the potential source areas (Q. Wang et al., 2016). Finally, cluster and CWT analyses were performed using a GIS-based TrajStat software developed by Wang et al. (2009).

2.7 The Optical Properties of Aerosols and Clouds (OPAC) Model

The OPAC model was used to retrieve the following parameters: aerosol optical depth (AOD), single scattering albedo (SSA), and asymmetric parameter (AP). The parameters were important in estimating the radiative effect of aerosols. A detailed description of the OPAC software package was given by Hess et al. (1998). The measured mass concentrations of OC, EC, and water-soluble ions as well as the estimated mineral dust loading (=[Fe]/0.035) during the day were used in the OPAC model to estimate the optical parameters. Moreover, the BC number concentration in the OPAC model was constrained by the measured EC mass concentration. Although several water-soluble ions and mineral dust were obtained, they did not contain all the water-soluble and insoluble material. Therefore, based on the measured data, the number concentrations of water-soluble and insoluble materials were tuned. This was done until the differences between the OPAC-derived light scattering, light absorption, and SSA versus the corresponding PAX-measured values were within 5% (Fig. S3). After the aerosol light extinction coefficient (sum of light scattering and absorption) was obtained, the AOD was estimated as follows (Hess et al., 1998):

删除了: **Cluster analysis**
删除了: s
删除了: for
删除了: m
删除了: based on
删除了: , which is defined as follows
删除了: :
删除了: by
带格式的: 标题 2

$$\mathrm{AOD} = \sum_j \int_{H_{j,min}}^{H_{j,max}} \sigma_{e,j}(h)dh = \sum_j \sigma_{e,j}^{1} N_j(0) \int_{H_{j,min}}^{H_{j,max}} e^{-\frac{h}{Z_j}} dh \quad (12)$$

where $H_{j,max}$ and $H_{j,min}$ were the upper and lower boundaries in layer j; $\sigma_{e,j}$ was the surface aerosol light extinction coefficient in layer j; h was the layer height; $\sigma_{e,j}^{1}$ represented the aerosol light extinction coefficient that was normalized to 1 particle cm^{-3}; N_j was the number concentration in layer j; and Z was the scale height. Furthermore, the OPAC-derived AODs were tuned to match the satellite-derived AODs (https://giovanni.gsfc.nasa.gov/giovanni, last access: January 2020) by altering the scale height in OPAC until the difference between them was within 5%. Owing to closure with AOD and anchoring of chemical composition, the assumptions in the OPAC model did not have a significant impact on the estimation of radiative effect in subsequent section 2.8 (Satheesh and Srinivasan 2006).

2.8 Estimations of radiative effect and heating rate

The LAC direct radiative effect (DRE) was estimated by the Santa Barbara DISORT (Discrete Ordinate Radiative Transfer) Atmospheric Radiative Transfer (SBDART) model in the shortwave spectral region of 0.25–4.0 μm. A detailed description of the SBDART model was given by Ricchiazzi et al. (1998). The AOD, SSA, and AP are essential input parameters in the SBDART model and were obtained from the OPAC model (see section 2.7). In addition to these, several other input parameters were included, namely the surface albedo, solar zenith angle, and profiles of atmospheric parameters. The surface albedo was derived from the Moderate Resolution Imaging Spectroradiometer (https://modis-atmos.gsfc.nasa.gov/ALBEDO/index.html, last access: January 2020). On the other hand, the solar zenith angle was calculated with a specific time and location (i.e., latitude and longitude) using a small code from the SBDART model. Furthermore, six standard atmospheric vertical profiles (i.e., tropical, mid-latitude summer, subarctic summer, mid-latitude winter, subarctic winter and US62) were embedded in the SBDART model. They provided vertical distributions of temperature, pressure, water vapor, and ozone density (Ricchiazzi et al., 1998). In this study, the mid-latitude summer was selected to represent the situation of Sanya based on its classification as a mid-latitude region. Obregón et al. (2015) demonstrated that the SBDART model could provide a reliable estimation of radiative effect. Moreover,

设置了格式: 英语(英国)

删除了: ↵

删除了: 7

删除了: forcing

删除了: forcing

删除了: F

删除了:

删除了:

删除了: The principle of

删除了: is described in detail in

aerosol DRE was defined as the difference in the radiation flux (F) either at the Earth's surface or at the top of the atmosphere, respectively with and without the aerosol in the atmosphere:

$$DRE = (F\downarrow - F\uparrow)_{\text{with aerosol}} - (F\downarrow - F\uparrow)_{\text{without aerosol}} \quad (13)$$

where ↓ and ↑ represented the downward and upward flux, respectively. Atmospheric DRE was then estimated by the difference between the DRE at the top of the atmosphere and the Earth's surface.

Further, the atmospheric heating rate ($\frac{\partial T}{\partial t}$, in unit of K d^{-1}) caused by LAC aerosols was estimated using the first law of thermodynamics and hydrostatic equilibrium as follows (Liou, 2002):

$$\frac{\partial T}{\partial t} = \frac{g}{C_p} \times \frac{\Delta F}{\Delta P} \quad (15)$$

where $\frac{g}{C_p}$ was the lapse rate and g stood for acceleration due to gravity while C_p described the specific heat capacity of air at a constant pressure (1006 J kg^{-1} K^{-1}); Additionally, ΔF was the atmospheric DRE contributed by LAC aerosols and ΔP represented the atmospheric pressure difference (300 hPa).

3 Results and discussion

3.1 Overview of Abs(λ)

The AE33 absorption was first corrected using PAX measurement and a strong correlation ($r = 0.96$, $p < 0.01$) between them was found (Fig. S4). A slope of 2.3 was regard as the correction factor and was comparable to the values of 2.0–2.6 reported by previous studies using a similar method (Qin et al., 2018; Tasoglou et al., 2017; Wang et al., 2019b). This difference may mainly be related to the matrix scattering and lensing effects. The time series of corrected Abs(λ) is shown in Fig. 1 and a statistical summary of the data presented in Table 1. The average Abs(λ) were 15.7 ± 5.3, 11.4 ± 3.7, 9.7 ± 3.0, 8.3 ± 2.6, 7.0 ± 2.2, and 4.9 ± 1.5 Mm^{-1} at 370, 470, 520, 590, 660, and 880 nm, respectively in the throughout the study. However, it is noteworthy that such single-wavelength calibrations may overestimate Abs(λ) at long wavelengths (i.e., λ = 590, 660, and 880 nm) and underestimate it at short wavelengths (i.e., λ = 370 and 470 nm) owing to the correction factor's dependence on wavelength (Kim et al., 2019). Compared to previous work, the Abs(λ) in this study were lower than those obtained from urban areas in China and Europe (J. Wang et al., 2018; Liakakou et al., 2020). However, they were comparable to some rural and

删除了: The measured mass concentrations of OC, EC, and water-soluble ions as well as the estimated dust loading (=[Fe]/0.035) during the daytime were used in the Optical Properties of Aerosol and Cloud (OPAC) model to estimate the single scattering albedo, aerosol optical depth, and asymmetric parameter. These are essential input parameters in SBDART model. More detailed description of the software package OPAC can be found in Hess et al. (1998). The light absorption, light scattering, and single scattering albedo measured by PAX were used to constrain the performance of OPAC, and small differences were found between modelled and measured values (Fig. [2]

删除了: is
删除了: , of which
删除了: represents
删除了: the
删除了: s
删除了: is
删除了: forcing
删除了: ;
删除了: s
删除了: Owing to the matrix scattering effect,
删除了: the
删除了: ,
删除了: was found
删除了: 3
删除了: The
删除了: , which is
删除了:
删除了:
删除了: in
删除了: After correction, t
删除了: during the campaign
删除了: (Fig. S4)
删除了: should be noted
删除了: while
删除了: wavelength dependence of
删除了: with
删除了: studies
下移了 [1]: (J. Wang et al., 2018; Liakakou et al., 2020;
删除了: Zanatta et al., 2016; Zhu et al., 2017)
删除了: here is
移动了(插入) [1]
删除了: ;
删除了: but

remote areas where anthropogenic activities were not intensive (Zanatta et al., 2016; Zhu et al., 2017). This suggests the possibility of a relatively small LAC burden in the atmosphere at Sanya during the study. Additionally, $Abs_{BC}(\lambda)$ contributed more than 77% to $Abs(\lambda)$ whereas the contribution of $Abs_{BrC}(\lambda)$ was less than 17% (Fig. 2). This was consistent with previous studies showing that BC was stronger at absorbing light compared to BrC at the near-ultraviolet to near-infrared wavelengths in the atmosphere (Massabò et al., 2015; Liakakou et al., 2020). However, laboratory studies reported that $Abs_{BrC}(\lambda)$ could exceed $Abs_{BC}(\lambda)$ at short wavelengths in fresh smoke from biomass burning, especially in the smoldering phase (Tian et al., 2019; Chow et al., 2018). Furthermore, the fraction of $Abs_{BC}(\lambda)$ increased with an increase in wavelength although the fraction of $Abs_{BrC}(\lambda)$ showed an inverse trend with a dramatic drop from 17% at 370 nm to 3% at 660 nm as shown in Fig. 2. This suggests a stronger light-absorbing capacity for BrC at short wavelengths compared to the long ones. With regard to the relationship between $Abs(\lambda)$ and carbonaceous composition, the $Abs_{BC}(\lambda)$ correlated well with EC mass concentration ($r = 0.93$, $p < 0.01$, Fig. S5). However, a weak but significant correlation was observed between $Abs_{BrC}(\lambda)$ and OC mass concentration ($r = 0.27–0.42$, $p < 0.05$, Fig. S6). The results further conformed that BC was the dominant light-absorbing material in LAC aerosols while OC comprised more of non-light-absorbing carbon components compared to the light-absorbing ones.

删除了：,…where the…anthropogenic activities are …ere not intensive (Zanatta et al., 2016; Zhu et al., 2017). This suggests a …he possibility of a relatively small LAC burden in the atmosphere at Sanya during the campaign ... [13]

删除了：From the perspective of LAC components, the …$bs_{BC}(\lambda)$ contributed more than 77% to $Abs(\lambda)$,…whereas the contribution of $Abs_{BrC}(\lambda)$ was less than 17% (Fig. 2S4…. This wasis…consistent with previous studies showing that BC wasis a…stronger at absorbing light absorber than…ompared to BrC from …t the near-ultraviolet to near-infrared wavelengths in the atmosphere (Massabò et al., 2015; Liakakou et al., 2020). However, laboratory studies reported that $Abs_{BrC}(\lambda)$ can …ould exceed $Abs_{BC}(\lambda)$ at short wavelengths in fresh smoke from biomass -…urning smokes… especially in thefor…smoldering phase (Tian et al., 2019; Chow et 2018). Furthermore, As shown in Fig. S4, …he fraction of $Abs_{BC}(\lambda)$ enhanced …ncreased with an increase inas the…wavelength increased, but…lthough the fraction of $Abs_{BrC}(\lambda)$ showed an inverse trend,…with a dramatical…dropping…from 17% at 370 nm to 3% at 660 nm as shown in Fig. 2. This,…suggestsing…a stronger light-absorbing capacity for BrC at short wavelengths compared to the than…long ones. With regard to the From …elationship between $Abs(\lambda)$ and carbonaceous composition (Fig. S5)… the $Abs_{BC}(\lambda)$ correlated well ($r = 0.93$, $p < 0.01$) …ith EC mass concentration ($r = 0.93$, $p < 0.01$, Fig. S5). However, while…a weak but significant correlation ($r = 0.27 – 0.42$, $p < 0.05$)…was observedfound…between $Abs_{BrC}(\lambda)$ and OC mass concentration ($r = 0.27–0.42$, $p < 0.05$, Fig. S6). The results further conformed that BC was the dominant light-absorbing material in LAC aerosols while OC comprised more of non-light-absorbing carbon components relative ... [14]

3.2 Source apportionment of $Abs(\lambda)$

To quantify the contributions of various sources to $Abs(\lambda)$, chemical species and $Abs_{pri}(\lambda)$ were simultaneously used as input parameters in the PMF5.0 model. Online $Abs_{pri}(\lambda)$ data was integrated to match each filter sampling time. The selected chemical species included carbonaceous matter (i.e., OC and EC), water-soluble cations (i.e., Na^+, K^+, and Ca^{2+}), elements (i.e., Ti, V, Mn, Fe, Ni, Cu, Zn, and Br), and hopanes. The mass concentrations of the chemicals are summarized in Table 2. Based on Eq. (5), $Abs_{sec}(\lambda)$ accounted for less than 5% of $Abs(\lambda)$ (Table S1), suggesting a negligible impact of secondary formation on the light absorption capacity of aerosols during the study. Therefore, the uncertainty caused by using only $Abs_{pri}(\lambda)$ in the model could be put to rest in the absence of an effective way to identify the sources of secondary BrC.

删除了：the …hemical species and $Abs_{pri}(\lambda)$ were used…simultaneously used as input parameters in the PMF5.0 model. Online $Abs_{pri}(\lambda)$ data was integrated to match each filter sampling time. The selected chemical species included carbonaceous matter (i.e., OC and EC), water-soluble cations (i.e., Na^+, K^+, and Ca^{2+}), elements (i.e., Ti, V, Mn, Fe, Ni, Cu, Zn, and Br), and hopanes., and…Tt…eir…mass concentrations of the chemicals are summarized in Table S1…. Based on Eq. (5), the …$bs_{sec}(\lambda)$ explained …ccounted for less than 5% of $Abs(\lambda)$ (Table S12…, suggesting a negligible impact of secondary formation on the light absorption capacity of aerosols during the campaign…tudy. Thus…herefore, the uncertainty caused by the only use of…sing only $Abs_{pri}(\lambda)$ in the model could be put to rest neglected …n the absence of an effective way to identify the sources of light absorption contributed by …econdary organic aerosol… ... [15]

Moreover, two to seven factors were selected to initiate the PMF5.0 run. Due to the additional factors, the Q/Q_{exp} ratio decreased with the increased number of factors as shown in Fig. S7. The decrease in Q/Q_{exp} was large when the factor number changed from 2 to 3 and 3 to 4 but stabilized as the factor number grew larger than 4, indicating that four factors may be the optimal solution. After multiple runs of the PMF5.0 model, four factor sources including ship emissions, motor vehicle emissions, biomass burning, and fugitive dust were finally identified (Fig. 3a). Additionally, the modeled $Abs_{pri}(\lambda)$ at different wavelengths showed strong correlations with the measured $Abs(\lambda)$ ($r = 0.82–0.89$, $p < 0.01$, Fig. S8). The slopes of 0.92–0.98 were consistent with the absorption fractions of $Abs_{pri}(\lambda)$ estimated by the BC-tracer method combined with the MRS approach (Table S1). The scaled residuals for each species varied between -3 and +3.

The uncertainty of each factor profile was further evaluated using BS, DISP, and BS-DISP. The BS results showed that the reproducibility of each source factor was larger than 80% (Table S2), indicating good stability. Therefore, this suggested that the four source factors were appropriate. No swaps occurred in DISP, indicating the stability of the selected solution. Furthermore, all BS-DISP runs were successful. Overall, these results pointed to the efficiency of the PMF5.0 model in performing optical source apportionment.

The first source factor was characterized by large proportions of V, Ni, and hopanes as well as moderate amounts of OC, EC, Na^+, K^+, Cu, and $Abs_{pri}(\lambda)$ as shown in Fig. 3a. V and Ni were associated with oil fuel combustion (Moreno et al., 2010), and their ratio (V/Ni) can be used to further identify ship engine emissions, which has a typical range of 2.5–4.0 (Cesari et al., 2014). The estimated V/Ni ratio was 3.4 in this source factor, consistent with the previously established range of ship engine emissions. Since hydrocarbons are the major components of ship engine oil, hopanes, OC, and EC can be produced as byproducts in the combustion process. Therefore, this source factor was assigned to ship emissions. The second source factor was associated with large amounts of Cu, Zn, and Br as well as moderate proportions of hopanes, EC, Ti, and $Abs_{pri}(\lambda)$. Previous studies confirmed that hopanes, Br, and EC were typically present in vehicle exhaust particles (Huang et al., 1994; Sheesley et al., 2009). Additionally, Zn and Cu were associated with lubricant and metal brake wear (Lin et al., 2015). Therefore, this source factor was allocated to motor vehicle emissions. The third source factor was dominated by high proportions of K^+,

删除了: of light absorption were identified,
删除了: mineral
删除了: 1
删除了: T
删除了: (r = 0.82 – 0.89, p < 0.01)
删除了: those
删除了: 6
删除了:
删除了:
删除了: 2
删除了: T
删除了: suggest a good performance
删除了: the
删除了: As shown in Fig. 1a, t
删除了: loadings
删除了: contributions
删除了: are
删除了: ,
删除了: the
删除了:
删除了:
删除了: feature
删除了: Because the
删除了: is
删除了: fuel
删除了: the
删除了: T
删除了: therefore
删除了: featured
删除了: loadings
删除了: contributions
删除了: have
删除了: consist
删除了: ,
删除了: and
删除了: are
删除了: the
删除了: us
删除了: contributions

OC, EC, and $Abs_{pri}(\lambda)$, which was an obvious feature of biomass burning (Forello et al., 2019). Finally, the fourth source factor was characterized by large amounts of several crustal materials such as Ca^{2+}, Ti, Fe, and Mn and was identified as mineral dust.

Notably, biomass burning occupied the largest proportion of light absorption ($Abs_{biomass}(\lambda)$) at 32–44% of $Abs_{pri}(\lambda)$ as shown in Fig. 3a. Sanya is coastal city with heavy maritime traffic (e.g., the cargo handling capacity was larger than 5.8 million tons in 2017 at Sanya port, http://tjj.sanya.gov.cn/tjjsite/2019nnj/tjnj.shtml, in Chinese) therefore absorption of ship emissions ($Abs_{ship}(\lambda)$) also had a significant contribution to $Abs_{pri}(\lambda)$ (30–39%). The contribution of motor vehicle emissions ($Abs_{vehicle}(\lambda)$ = 17–24% of $Abs_{pri}(\lambda)$) was much lower than that of biomass burning and ship emissions. Moreover, the absorption of fugitive dust ($Abs_{dust}(\lambda)$) occupied less than 10% of $Abs_{pri}(\lambda)$, consistent with previous reports where it was identified as a minor contributor in the atmosphere (Yang et al., 2009; Zhao et al., 2019). This small absorptive fraction may be attributed to the low proportion of light-absorbing iron oxides in the atmosphere. Furthermore, the $Abs_{pri}(\lambda)$ of different sources all decreased with the increased wavelength (Fig. 3b) although their relative contributions displayed distinct trends (Fig. 3a). The fraction of $Abs_{ship}(\lambda)$ and $Abs_{vehicle}(\lambda)$ increased with an increase in wavelength while a reverse trend was observed in the $Abs_{biomass}(\lambda)$ fraction. This discrepancy can be explained by the large amount of BrC present in biomass-burning emissions which can result in more light absorption at short wavelengths relative to the long ones.

To identify the possible source areas that affected $Abs_{pri}(\lambda)$, CWT analysis was performed based on the three-day backward trajectories. Large CWT values were mainly concentrated in the South China Sea (Fig. S9), highlighting the effect of ship emissions on aerosol light absorption. Additionally, the three-day backward trajectories were grouped into four cluster-mean trajectories to investigate the impact of different sources on $Abs_{pri}(\lambda)$ (Fig. 4). The air masses associated with Cluster #1 originated from the South China Sea. The $Abs_{ship}(\lambda)$ was the largest contributor in this cluster, constituting 44–45% of $Abs_{pri}(\lambda)$ due to the high vessel traffic density over the South China Sea, consistent with the CWT results. Cluster #1 accounted for about 44% of the total trajectories, suggesting that Sanya was subjected to the influence of ship exhaust-related LAC aerosols transported from the South China Sea. It is noteworthy that the diurnal pattern of $Abs_{pri}(\lambda)$ showed typically high values in the mornings and evenings (Fig. S10). This

删除了：,…which was an obvious feature of biomass burning (Forello et al., 2019). Finally, tT…e fourth source factor was characterized by large amountsloadings…of several crustal materials,…such as Ca^{2+}, Ti, Fe, and Mn,…and, therefore, it ... [16]

删除了：As shown in Fig. 1b… biomass burning occupied was …he largest proportion of light absorption ($Abs_{biomass}(\lambda)$) contributor …ton average, constituting…32 … …4% of $Abs_{pri}(\lambda)$ as shown in Fig. 3a. Sanya isAs a…coastal city with heavy maritime traffic (e.g., the handling capacity was larger than 5.8 million tons in 2017 at Sanya port, http://tjj.sanya.gov.cn/tjjsite/2019nnj/tjnj.shtml, in Chinese) therefore absorption of,…ship emissions ($Abs_{ship}(\lambda)$)also…also had a significant contributioned significantly…to $Abs_{pri}(\lambda)$ (30 … …9%). The contribution of motor vehicle emissions ($Abs_{vehicle}(\lambda)$ = 17 … …4% of $Abs_{pri}(\lambda)$) was much lower than that of biomass burning and ship emissions. Moreover, the absorption of fugitive mineral …ust ($Abs_{dust}(\lambda)$) explained …ccupied less than 10% of $Abs_{pri}(\lambda)$, consistent with previous reports where it was identified as as role of…minor contributorion…in the atmosphere (Yang et al., 2009; Zhao et al., 2019). This small absorptiveon…fraction may be mainly …ttributed to the low content …roportion of light-absorbing iron oxides in the atmosphere. FurthermoreAs shown in Fig. 1c… the $Abs_{pri}(\lambda)$ of different sources all decreased with the increased wavelength (Fig. 3b) although, but…their relative contributions exhibited …isplayed distinct trends (Fig. 3a). The absorption …ractions…of $Abs_{ship}(\lambda)$ and $Abs_{vehicle}(\lambda)$ increasedship and motor vehicle emissions enhanced…with an increase in as the…wavelength increased…while a reverse trend was observed for biomass burning…n the $Abs_{biomass}(\lambda)$ fraction. This discrepancy can explained by the large amount of BrC existed …resent in biomass-burning emissions,…which can result in more light absorption at short wavelengths relative to the long ones (see Fig. S4) ... [17]

删除了：To investigate the impacts of regional transport on $Abs_{pri}(\lambda)$, …hree-day backward trajectories were grouped into four cluster-mean trajectories to investigate the impact of different sources on $Abs_{pri}(\lambda)$ (Fig. 42…. The air masses associated with Cluster #1 derived …riginated from the South China Sea. The $Abs_{ship}(\lambda)$ was With a high vessel traffic density over the South China Sea, ship emissions are …he largest contributor in this cluster,…constituting 44 … …5% of $Abs_{pri}(\lambda)$ due to the high vessel traffic density over the South China Sea, consistent with the CWT results. Cluster #1 accounted for aboutThis cluster comprised…44% of the total trajectories, suggesting that Sanya was often …ubjected to the influences… ... [18]

was attributed to the daily anthropogenic activities and variations in height of the planetary boundary layer. Given that the air masses from the South China Sea are unable to carry pollutants from biomass burning, motor vehicles, and fugitive dust, these sources were possibly mainly influenced by local emissions.

Cluster #2 originated from the South China Sea near the Indochina Peninsula and accounted for 35% of the total trajectories. The $Abs_{ship}(\lambda)$ was also vital in this cluster, accounting for 34–37% of $Abs_{pri}(\lambda)$. Fig. S10 shows that the $Abs_{pri}(\lambda)$ of Cluster #2 displayed a similar diurnal trend as that of Cluster #1. Considering that the air masses of Cluster #2 also originated from the South China Sea, the sources except for ship emissions were mainly influenced by local discharge. A small number of air masses were grouped into Cluster #3 and Cluster #4, accounting for only 6% and 15% of total trajectories, respectively. Cluster #3 originated from southern Burma and passed over Thailand, Laos, and Vietnam. On the other hand, Cluster #4 had the longest cluster-mean trajectory which originated and passed through the coastal areas of South-eastern China. Biomass burning was the dominant contributor to $Abs_{pri}(\lambda)$ in both clusters, with 62–69% for Cluster #3 and 56–64% for Cluster #4. Moreover, the $Abs_{biomass}(\lambda)$ of Cluster #3 and Cluster #4 were 1.8–4.4 times higher than those of Cluster #1 and Cluster #2. Since the $Abs_{biomass}(\lambda)$ from Cluster #1 and Cluster #2 were mainly attributed to local emissions, the higher values in Cluster #3 and Cluster #4 may have been influenced by the long-range transport of biomass burning from Southeast Asia and South-eastern China, where there was a large number of fire incidences (Fig. 4).

3.3 Source-dependent optical properties of LAC aerosol

According to a power law function (Fig. 5), the average LAC AAE (1.4, Table 1) was greater than unity during the study, indicating the presence of both BC and BrC in the atmosphere. In addition, the estimated AAE of motor vehicle emissions ($AAE_{vehicle}$) was 0.96. This was close to the previously reported range of 0.9–1.1, obtained from ambient observations using the radiocarbon method or vehicle exhaust-related source experiments (Sandradewi et al., 2008; Chow et al., 2018; Zotter et al., 2017). This narrow range of $AAE_{vehicle}$ obtained by various studies suggests that the spectral dependence of vehicle exhaust-related LAC absorption was less affected by atmospheric processes. Furthermore, the AAE of ship emissions (AAE_{ship} = 1.06) was similar to that of $AAE_{vehicle}$. These low spectral dependences of light absorption

删除了: , which contained
删除了: Ship emissions were
删除了:
删除了:
删除了: However, owing to the large burden of biomass-burning-related carbonaceous aerosol in Southeast Asia (Li et al., 2017), biomass burning contributed more to $Abs_{pri}(\lambda)$ (36 – 43%) than ship emissions. This can be further confirmed by numerous fire counts observed in Vietnam (Fig. 2), which is near the origination area of Cluster #2.
删除了: S
删除了: comprising
删除了: derived
删除了: , where there were intensive biomass-burning activities (Fig. 2)….
删除了: s
删除了: For these two clusters, b
删除了:
删除了:
删除了:
删除了:
删除了: Retrieved from
删除了: campaign
删除了: (Fig. 3)
删除了: As shown in Fig. 3
删除了: 1.0
删除了: ,
删除了: ing
删除了: values (
删除了:
删除了:
删除了:)
删除了: and the
删除了: among
删除了: is
删除了: T
删除了: 1
删除了: showed a similarity with

indicate that BC was the dominant compound in LAC aerosols from ship and motor vehicle emissions. Compared to marine engine emissions, the AAE_{ship} obtained in this study was consistent with the values derived from marine gas oil and diesel fuel emissions (1.0 ± 0.1) but was lower than heavy fuel oil exhaust (1.7 ± 0.2) (Corbin et al., 2018). This indicates that Sanya may be influenced more by ships using distillate rather than heavy fuel oil.

The AAE of biomass burning ($AAE_{biomass}$ = 1.75) was larger than that from ship and motor vehicle emissions. This implyed the presence of BrC in LAC aerosols derived from biomass-burning in addition to BC. The observation corroborated with previous studies which showed that BrC was mainly derived from biomass burning rather than fossil fuels in the atmosphere (Laskin et al., 2015). Additionally, chamber studies showed that the AAEs of fresh smoke from biomass burning varied largely (e.g., 1.64–3.25) depending on the type of biomass and their burning efficiencies (Tian et al., 2019). The $AAE_{biomass}$ from this study was close to those (1.7–1.9) from the atmosphere constrained by the radiocarbon method (Sandradewi et al., 2008; Zotter et al., 2017). Given that the approach used in this study could retrieve the source-specific AAEs in the atmosphere, it can also improve the performance of those optical source apportionment models based solely on optical data.

Owing to the dominance of BC in ship and motor vehicle emissions, only $MAC_{BC}(\lambda)$ was estimated for these two sources. The results of optical source apportionment revealed that the estimated $MAC_{BC}(\lambda)$ of motor vehicle emissions ($MAC_{BC,vehicle}(\lambda)$) were close to the values of uncoated BC particles at different wavelengths (Fig. 6). This indicated that vehicle exhaust-related BC particles were mainly associated with local emissions and underwent minor atmospheric aging processes. In contrast, the $MAC_{BC}(\lambda)$ of ship emissions ($MAC_{BC,ship}(\lambda)$) was 1.4–1.6 times larger than that of the uncoated ones (Fig. 6). This implied that ship exhaust-related BC particles were prone to substantial aging during transit from the ocean. Freshly emitted BC particles from fossil fuels tend to mix externally with other substances and become internally-mixed ones after aging (Xing et al., 2020). It was therefore unexpected for the obtained $MAC_{BC,ship}(\lambda)$ to have a similar value as that of marine engine emissions reported by Corbin et al. (2018) (7.8 $m^2\ g^{-1}$ at 780 nm, extrapolated to the same wavelengths in this study by assuming an AAE_{BC} = 1.1). Consequently, more work is needed to understand the large $MAC_{BC}(\lambda)$ values from marine engine emissions.

删除了: contributor to …AC aerosols from in…ship and motor vehicle emissions. Compared to marine engine emissions, the AAE_{ship} obtained in this study is …as consistent with the values derived from marine gas oil and diesel fuel emissions (1.0 ± 0.1) but was lower than heavy fuel oil exhaust (1.7 ± 0.2) (Corbin et al., 2018). This indicates comparison reflects …hat Sanya may be influenced more likely influenced …y those …hips using distillate fuels…relative to ... [19]

删除了: 8… was larger than those …hat from ship and motor vehicle emissions. This,…implyeding…the presence of BrC in biomass-burning-related …AC aerosols derived from biomass-burning in addition to BC. The observation corroboratedThis is consistent…with previous studies which showeding…that BrC wasis…mainly derived from biomass burning rather than fossil fuels in the atmosphere (Laskin et al., 2015). Additionally,Although…chamber studies have shown…howed that the AAEs of fresh smoke from biomass -…urning smokes…variedy…largely (e.g., 1.64 … ….25) depending on the types…of biomass and their burning efficiencies (Tian et al., 2019).,…Tt…e $AAE_{biomass}$ in …rom this study is…as close to those (1.7 … ….9) fromin…the atmosphere constrained by the radiocarbon method (Sandradewi et al., 2008; Zotter et al., 2017). Given that As our…he approach used in this study couldcan…retrieve the source-specific AAEs in the atmosphere, it can also improve the performance of those optical source apportionment models that …aseds on… ... [20]

删除了: Based on t…he results of optical source apportionment revealed that,…the estimated $MAC_{BC}(\lambda)$ of motor vehicle emissions ($MAC_{BC,vehicle}(\lambda)$) were close to the values of uncoated BC particles at different wavelengths (Fig. 64…. This indicateds…that vehicle exhaust-related BC particles were mainly associated with local emissions and underwent experienced…minor atmospheric aging processes. By …n contrast, the $MAC_{BC}(\lambda)$ of ship emissions ($MAC_{BC,ship}(\lambda)$) was 1.4 … ….6 times larger than that of the uncoated ones (Fig. 64…. This,…impliedying…that ship exhaust-related BC particles were subject …rone to substantial aging during transittheir transport…from the ocean. Freshly emitted BC particles from fossil fuels tend to mix externally with other substances and become internally-mixed ones after aging (Xing et al., 2020). It is…as therefore unexpected for the obtainedthat our…$MAC_{BC,ship}(\lambda)$ to have a is …imilar to the…value as that of marine engine emissions reported by Corbin et al. (2018) (7.8 $m^2\ g^{-1}$ at 780 nm, extrapolated to the same wavelengths of …n this study by assuming an AAE_{BC} = 1.1) (Corbin et al., 2018), because freshly emitted fossil fuel BC particles tend to be externally-mixed with other substances and become internally-mixed ones after aging (Xing et al., 2020)… Actually…onsequently, the authors of that study also recognize more work is needed to clarify …nderstand their ambiguous…large $MAC_{BC}(\lambda)$ values from of ... [21]

Since LAC aerosols derived from biomass burning comprised of both BC and BrC, the $MAC_{BC}(\lambda)$ and $MAC_{BrC}(\lambda)$ were retrieved based on the results of optical source apportionment. The findings revealed that the $MAC_{BC}(\lambda)$ of biomass burning ($MAC_{BC,biomass}(\lambda)$) was larger than $MAC_{BC,vehicle}(\lambda)$ as shown in Fig. 6. This was consistent with previous studies showing a stronger capacity to absorb light by BC from biomass burning compared to that from motor vehicle emissions (Qiu et al., 2014; Q. Wang et al., 2018b). Moreover, the $MAC_{BC,biomass}(\lambda)$ was smaller than $MAC_{BC,ship}(\lambda)$, suggesting a stronger ability to absorb light by BC particles from ship exhaust. A broader implication of this observation is that more focus should be put on BC particles related to ship emissions due to their impact on climate given the increase in shipping activities globally.

The $MAC_{BrC}(\lambda)$ of biomass burning ($MAC_{BrC,biomass}(\lambda)$) was highly dependent on wavelength, with 0.9 $m^2\ g^{-1}$ at λ = 370 nm but dropped close to zero (0.02 $m^2\ g^{-1}$) at λ = 660 nm (Fig. 6). Additionally, the $MAC_{BrC,biomass}(\lambda)$ was several times to two orders of magnitude lower than $MAC_{BC}(\lambda)$ from different sources, suggesting that BC had a stronger ability to absorb light compared to BrC. Notably, the $MAC_{BrC}(\lambda)$ obtained in this study lied within the range reported by previous investigations although with differences among studies (Wang et al., 2019b; Cho et al., 2019). The differences in $MAC_{BrC}(\lambda)$ may partly be related to biomass types and their burning efficiencies as well as the aging processes of BrC in the atmosphere. In addition, the use of different BrC substitutes (e.g., OM, organic aerosol, or water-soluble organic carbon) may have impacted the calculation of $MAC_{BrC}(\lambda)$. Compared to previous laboratory studies, the $MAC_{BrC,biomass}(\lambda)$ obtained here was smaller than that of fresh smoke from biomass burning (Zhong and Jang, 2014; Pandey et al., 2016). Given that photobleaching is an effective way of turning BrC into a transparent organic substance (Laskin et al., 2015), the smaller atmospheric $MAC_{BrC,biomass}(\lambda)$ observed in this study may be attributed to the elimination of organic chromophores induced by the bright sunlight at Sanya.

The MAC links LAC mass to its light absorption, which is an important parameter in climate models to evaluate global or regional LAC radiative effects. Because identifying source-specific MACs still remains challenging in the atmosphere, an equal MAC of different sources is often assumed in climate models (Bond et al., 2013). However, this assumption could cause a large uncertainty owing to the distinct MACs for various sources (e.g., $MAC_{BC,ship}(\lambda) > MAC_{BC,biomass}(\lambda) > MAC_{BC,vehicle}(\lambda)$ in this study). The chemical

删除了: As biomass-burning-related …AC aerosols derived from biomass burning comprised of both BC and BrC, the $MAC_{BC}(\lambda)$ and $MAC_{BrC}(\lambda)$ were retrieved based on the results of optical source apportionment (Fig. 4)… The findings revealed that the $MAC_{BC}(\lambda)$ of biomass burning ($MAC_{BC,biomass}(\lambda)$) was larger than $MAC_{BC,vehicle}(\lambda)$ as shown in Fig. 6. This was,…consistent with previous studies showing a stronger capacity to absorbBC…light by BC from absorption capacity for …iomass burning relative …ompared to that from motor vehicle emissions (Qiu et al., 2014; Q. Wang et al., 2018b). Compared with ship emissions…oreover, the $MAC_{BC,biomass}(\lambda)$ was smaller than $MAC_{BC,ship}(\lambda)$, suggesting a stronger ability to absorb light-absorbing ability for ship exhaust-related…by BC particles from ship exhaust. A broader implication of this observation is that more focus should be put on the impacts of ship emission-related …C particles related to ship emissions due to their impact on climate given the should be paid more attention owing to the striking ... [22]

删除了: wavelength …ependent on wavelength, with 0.91.7…$m^2\ g^{-1}$ at λ = 370 nm but dropped closeing…to near…zero (0.024…$m^2\ g^{-1}$) at λ = 660 nm (Fig. 64.… Additionally, tT…e $MAC_{BrC,biomass}(\lambda)$ was several times to two orders of magnitude lower than $MAC_{BC}(\lambda)$ of …rom different sources, suggesting that BC had an absolute…stronger ability to light …bsorb lighter for BC relative…compared to BrC. Notably, tT…e $MAC_{BrC}(\lambda)$ obtained in this study lied withhere is …n the range reported by previous investigations although with differences was found …mong studies (Wang et al., 2019b; Cho et al., 2019). This …he discrepancy of…ifferences in $MAC_{BrC}(\lambda)$ mayis…partly beially…related to biomass types and their burning efficiencies as well as the following …ging processes of BrC in the atmosphere. In addition, the use of different BrC substitutes (e.g., OMC… organic aerosol, or water-soluble organic carbon) is …ay have impacted the calculation ofalso a cause affecting…$MAC_{BrC}(\lambda)$ calculation… Compared previous laboratory studies, our …he $MAC_{BrC,biomass}(\lambda)$ obtained here wasis…smaller than those …hat offrom…fresh smoke from biomass -…urning smokes…(Zhong and Jang, 2014; Pandey et al., 2016). Given thatAs…photobleaching is an effective way to …f turning BrC into a transparent organic substance (Laskin et al., 2015), the smaller atmospheric $MAC_{BrC,biomass}(\lambda)$ observed in this studyhere ... [23]

composition-based optical source apportionment approach may provide a potential solution to resolve this issue, although more source-specific MACs in different areas and seasons are needed in the future study to gauge the accuracy of climate models. Moreover, this approach also can minimize the uncertainties of BC source apportionment using the aethalometer model due to the assumption of equal AAE and MAC of different sources.

3.4 Impacts of LAC aerosols on radiative effect

Fig. 7 shows the source-specific LAC DRE during the study. The LAC DRE varied from -5.5 to -1.6 W m^{-2} at the Earth's surface with an average cooling effect of -3.2 ± 1.0 W m^{-2}. In contrast, the LAC aerosols produced a warm effect of +1.5 ± 0.5 W m^{-2} at the top of the atmosphere with a range of +0.8 to +2.8 W m^{-2} suggesting a net energy gain. The presence of LAC aerosols enhanced aerosol DRE at the top of the atmosphere by 62% compared to the results of light scattering by aerosols only. Moreover, the difference between LAC DRE at the top of the atmosphere and the Earth's surface gave the atmospheric DRE (a net atmospheric absorption) of +4.7 ± 1.5 W m^{-2} and could generate a heating rate of 0.13 ± 0.04 K day^{-1}. With regard to LAC absorption sources, biomass burning was the largest contributor to LAC DRE at -1.5 ± 0.5 W m^{-2} and +0.7 ± 0.2 W m^{-2} on the surface of the Earth and the top of the atmosphere, respectively. In addition, BrC from biomass burning had a less contribution to LAC DRE compared to BC from the same source. However, the presence of BrC reinforced the LAC DRE of biomass burning by 21% as opposed to BC only, suggesting a substantial radiative effect from BrC aerosol. Additionally, the LAC DRE were -1.1 ± 0.4 W m^{-2} and +0.5 ± 0.2 W m^{-2} for ship emissions and -0.6 ± 0.2 W m^{-2} and +0.3 ± 0.1 W m^{-2} for motor vehicle emissions on the Earth's surface and the top of the atmosphere, respectively. The LAC DRE contributed by ship and motor vehicle emissions was mainly caused by BC aerosol. Although a larger BC atmospheric DRE was observed for biomass burning, ship emissions showed an equivalent capacity of radiative effect (0.5 (W m^{-2}) (μg m^{-3})$^{-1}$) from per unit BC mass concentration generating atmospheric DRE. In contrast, motor vehicle emissions had a smaller value of 0.3 (W m^{-2}) (μg m^{-3})$^{-1}$. Furthermore, the atmospheric heating rate of LAC aerosols was similar for biomass burning (0.06 ± 0.02 K day^{-1}) and ship emissions (0.05 ± 0.01 K day^{-1}) but larger than that produced by motor vehicle emissions

删除了: **forcing**
删除了: 5
删除了: F
删除了: campaign
删除了: F
删除了: ,
删除了: ,
删除了: forcing
删除了: with
删除了: T
删除了: F
删除了: forcing
删除了: ,
删除了: which can
删除了: From the perspective of
删除了: F, which were
删除了: at
删除了: 's surface
删除了: Although the
删除了: -
删除了: BrC contributed
删除了: F than that produced by
删除了: ,
删除了: strengthened
删除了: biomass-burning
删除了: forcing
删除了: relative
删除了: the result with
删除了: T
删除了: F
删除了: at
删除了: F
删除了: forcing
删除了: found
删除了: the
删除了: forcing production
删除了: forcing
删除了: By
删除了: ,

(0.03 ± 0.01 K day^{-1}). This further highlighted the importance of LAC aerosols from ship exhaust in atmospheric heating.

删除了：,…further indicating …ighlighted the importance of ship exhaust …AC aerosols from ship exhaust in atmospheric heating effect… ... [24]

4 Conclusions

In this study, the optical properties and radiative effect of LAC aerosols in Sanya, a Chinese tropical marine monsoon climate zone, were explored. The study found that light absorption caused by primary emissions was the mian contributor to LAC absorption while secondary processes played a minor role. Moreover, BC aerosol (> 77%) contributed more to $Abs_{LAC}(\lambda)$ compared to BrC (< 17%). Through a combination of chemical species and multi-wavelength absorption in a positive matrix factorization model, it was shown that biomass burning had the highest contribution to $Abs_{pri}(\lambda)$ (32–44%), followed by ship (30–39%) and motor vehicle emissions (17–24%). Fugitive dust had the lowest contribution (< 10%). Furthermore, cluster analysis of three-day backward trajectories showed that ship emissions were the major contributors to $Abs_{pri}(\lambda)$ when the air-masses originated from the South China Sea, whereas biomass burning dominated in other directions.

删除了：we explored …he optical properties and radiative forcing …ffect of light-absorbing carbonaceous (…AC)…aerosols in Sanya, a Chinese at a…tropical marine monsoon climate zone, were explored of China… The study found thatDuring the campaign, the…light absorption caused by primary emissions ($Abs_{pri}(\lambda)$) …as the dominant …ian contributor to LAC absorption ($Abs_{LAC}(\lambda)$) …hile minor contribution was found for…secondary processes played a role. Moreover, From the perspective of LAC composition, black carbon (…C)…aerosol (> 77%) contributed more to $Abs_{LAC}(\lambda)$ than …ompared to brown carbon (…rC)…(< 17%). Through a combination ofCoupling…chemical species andwith…multi-wavelength absorption in a positive matrix factorization model, it was shown we obtained …hat biomass burning had contributed …he highest contribution to $Abs_{pri}(\lambda)$ (32 … …4%),…followed by ship (30 … …9%) and motor vehicle emissions (17 … …4%). Fugitive dust had the lowest contribution, with the smallest for mineral dust…(< 10%). Furthermore, Based on the results of …luster analysis of three-day backward trajectories showed that,…ship emissions were became …he largest …ajor contributors to $Abs_{pri}(\lambda)$ when the air-masses originated from the South China Sea, ... [25]

Moreover, source-specific AAE showed a similarity between ship and motor vehicle emissions (1.06 versus 0.96). The low spectral dependence of light absorption indicated that LAC aerosols were dominated by BC in ship and motor vehicle emissions. In contrast, a large AAE of 1.75 was found in biomass burning, indicating the presence of both BC and BrC. Additionally, source-specific MAC showed that BC particles from ship emissions had the strongest light-absorbing capacity, followed by biomass burning and motor vehicle emissions. Compared to BC MAC, the BrC MAC of biomass burning was smaller with a value of 0.9 m^2 g^{-1} at λ = 370 nm but dropped to 0.02 m^2 g^{-1} at λ = 660 nm. The radiative transfer model also showed that the atmospheric DRE caused by LAC aerosols was +4.7 ± 1.5 W m^{-2} during the study and corresponded to a heating rate of 0.13 ± 0.04 K day^{-1}. The presence of BrC reinforced the LAC DRE of biomass burning by 21% as compared to BC only. Finally, ship emissions showed an equivalent capacity to produce radiative effect (0.5 (W m^{-2}) (μg m^{-3})$^{-1}$) from per unit BC mass concentration generating atmospheric DRE. In contrast, motor vehicle emissions had a smaller value of 0.3 (W m^{-2}) (μg m^{-3})$^{-1}$.

删除了：The …ource-specific absorption Ångström exponent (…AE)…showed a similarity between ship and motor vehicle emissions (1.061…versus 0.961.0…. The low spectral dependence of light absorption indicateds…that LAC aerosols werewas…dominated by BC in ship and motor vehicle emissions. By …n contrast, a large AAE of 1.758…was found for …n biomass burning, indicating the presence of both BC and BrC. Additionally, The …ource-specific mass absorption cross section (…AC)…showed that BC particles from ship emissions had the strongest light-absorbing capacity,…followed by biomass burning and motor vehicle emissions. Compared with …o BC MAC, the BrC MAC of biomass burning was smaller,…with a value of 0.91.7…m^2 g^{-1} at λ = 370 nm but droppeding…to 0.024…m^2 g^{-1} at λ = 660 nm. The radiative transfer model also showeds…that the atmospheric forcing …RE caused by LAC aerosols was +4.7 ± 1.5 W m^{-2} during the campaign,…tudy and which…correspondeds…to a heating rate of ± 0.04 K day^{-1}. The presence of BrC reinforcedstrengthened…the biomass-burning …AC forcing …RE of biomass burning by 21% as comparedrelative…to the result with …C only. Finally,The…ship emissions showed an equivalent capacity of…o produce radiative forcing production…ffect (0.5 (W m^{-2}) (μg m^{-3})$^{-1}$) from per unit BC mass concentration generating atmospheric forcing…RE. By ... [26]

Data availability. All data described in this study are available upon request from the corresponding authors.

Supplement. The supplement related to this article is available online.

Author contributions. QW, JC, and YH designed the campaign. PW and YZ provided the observation site and assisted with field sampling and measurements. WD and TZ conducted the chemical analyses. HL ran the PMF5.0 and SBDART model. JT performed the cluster analysis of air-mass trajectories. WZ provided the ArcGIS maps. QW conducted the data analysis and wrote the article with input from all co-authors.

Competing interests. The authors declare that they have no conflict of interest.

Acknowledgments. This work was supported by the Strategic Priority Research Program of Chinese Academy of Sciences (XDB40000000), the Youth Innovation Promotion Association of the Chinese Academy of Sciences (2019402), the Hainan Natural Science Foundation High-level Talent Project (2019RC243), and the Science and Technology Cooperation Project of Sanya (2018YD14 and 2012YD38).

删除了: 3

删除了: 2

References

Andreae, M. O., and Gelencsér, A.: Black carbon or brown carbon? The nature of light-absorbing carbonaceous aerosols, Atmos. Chem. Phys., 6, 3131-3148, https://doi.org/10.5194/acp-6-3131-2006, 2006.

Bond, T. C., Doherty, S. J., Fahey, D. W., Forster, P. M., Berntsen, T., DeAngelo, B. J., Flanner, M. G., Ghan, S., Kärcher, B., Koch, D., Kinne, S., Kondo, Y., Quinn, P. K., Sarofim, M. C., Schultz, M. G., Schulz, M., Venkataraman, C., Zhang, H., Zhang, S., Bellouin, N., Guttikunda, S. K., Hopke, P. K., Jacobson, M. Z., Kaiser, J. W., Klimont, Z., Lohmann, U., Schwarz, J. P., Shindell, D., Storelvmo, T., Warren, S. G., and Zender, C. S.: Bounding the role of black carbon in the climate system: A

scientific assessment, J. Geophys. Res.-Atmos., 118, 5380-5552, https://doi.org/10.1002/jgrd.50171, 2013.

Brown, S. G., Eberly, S., Paatero, P. and Norris, G. A.: Methods for estimating uncertainty in PMF solutions: Examples with ambient air and water quality data and guidance on reporting PMF results, Sci. Total Environ., 518–519, 626–635, https://doi.org/10.1016/j.scitotenv.2015.01.022, 2015.

Cesari, D., Genga, A., Ielpo, P., Siciliano, M., Mascolo, G., Grasso, F. M., and Contini, D.: Source apportionment of $PM_{2.5}$ in the harbour–industrial area of Brindisi (Italy): Identification and estimation of the contribution of in-port ship emissions, Sci. Total Environ., 497-498, 392-400, https://doi.org/10.1016/j.scitotenv.2014.08.007, 2014.

Cho, C., Kim, S.-W., Lee, M., Lim, S., Fang, W., Gustafsson, Ö., Andersson, A., Park, R. J., and Sheridan, P. J.: Observation-based estimates of the mass absorption cross-section of black and brown carbon and their contribution to aerosol light absorption in East Asia, Atmos. Environ., 212, 65-74, https://doi.org/10.1016/j.atmosenv.2019.05.024, 2019.

Chow, J. C., Watson, J. G., Chen, L. W. A., Chang, M. C. O., Robinson, N. F., Trimble, D., and Kohl, S.: The IMPROVE_A temperature protocol for thermal/optical carbon analysis: Maintaining consistency with a long-term database, J. Air Waste Manage. Assoc., 57, 1014-1023, https://doi.org/10.3155/1047-3289.57.9.1014, 2007.

Chow, J. C., Watson, J. G., Green, M. C., Wang, X., Chen, L. W. A., Trimble, D. L., Cropper, P. M., Kohl, S. D., and Gronstal, S. B.: Separation of brown carbon from black carbon for IMPROVE and Chemical Speciation Network $PM_{2.5}$ samples, J. Air Waste Manage. Assoc., 68, 494-510, https://doi.org/10.1080/10962247.2018.1426653, 2018.

Corbin, J. C., Pieber, S. M., Czech, H., Zanatta, M., Jakobi, G., Massabò, D., Orasche, J., El Haddad, I., Mensah, A. A., Stengel, B., Drinovec, L., Mocnik, G., Zimmermann, R., Prévôt, A. S. H., and Gysel, M.: Brown and black carbon emitted by a marine engine operated on heavy fuel oil and distillate fuels: Optical properties, size distributions, and emission factors, J. Geophys. Res.-Atmos., 123, 6175-6195, https://doi.org/10.1029/2017JD027818, 2018.

Draxler, R. R., and Rolph, G. D.: HYSPLIT (HYbrid Single-Particle Lagrangian Integrated Trajectory), Silver Spring, MD, Model access via NOAA ARL READY Website: http://www.arl.noaa.gov/ready/hysplit4.htmlNOAAAirResourcesLaboratory (last access: November 2019), 2003.

Drinovec, L., Močnik, G., Zotter, P., Prévôt, A. S. H., Ruckstuhl, C., Coz, E., Rupakheti, M., Sciare, J., Müller, T., Wiedensohler, A., and Hansen, A. D. A.: The "dual-spot" Aethalometer: an improved measurement of aerosol black carbon with real-time loading compensation, Atmos. Meas. Tech., 8, 1965-1979, https://doi.org/10.5194/amt-8-1965-2015, 2015.

Forello, A. C., Bernardoni, V., Calzolai, G., Lucarelli, F., Massabò, D., Nava, S., Pileci, R. E., Prati, P., Valentini, S., Valli, G., and Vecchi, R.: Exploiting multi-wavelength aerosol absorption coefficients in a multi-time resolution source apportionment study to retrieve source-dependent absorption parameters, Atmos. Chem. Phys., 19, 11235-11252, https://doi.org/10.5194/acp-19-11235-2019, 2019.

Healy, R. M., Sofowote, U., Su, Y., Debosz, J., Noble, M., Jeong, C. H., Wang, J. M., Hilker, N., Evans, G. J., Doerksen, G., Jones, K., and Munoz, A.: Ambient measurements and source apportionment of fossil fuel and biomass burning black carbon in Ontario, Atmos. Environ., 161, 34-47, https://doi.org/10.1016/j.atmosenv.2017.04.034, 2017.

Hess, M., Koepke, P., and Schult, I.: Optical Properties of Aerosols and Clouds: The Software Package OPAC, Bull. Amer. Meteorol. Soc., 79, 831-844, https://doi.org/10.1175/1520-0477(1998)079<0831:OPOAAC>2.0.CO;2, 1998.

Huang, X., Olmez, I., Aras, N. K., and Gordon, G. E.: Emissions of trace elements from motor vehicles: Potential marker elements and source composition profile, Atmos. Environ., 28, 1385-1391, https://doi.org/10.1016/1352-2310(94)90201-1, 1994.

IPCC: Climate Change 2013: The Physical Science Basis, Cambridge University Press, Cambridge, UK and New York, NY, USA, 2013.

Kim, J.-H., Kim, S.-W., Ogren, J. A., Sheridan, P. J., Yoon, S.-C., Sharma, S., and Lin, N.-H.: Multiple scattering correction factor estimation for aethalometer aerosol absorption coefficient measurement, Aerosol Sci. Technol., 53, 160-171, https://doi.org/10.1080/02786826.2018.1555368, 2019.

Küpper, M., Quass, U., John, A. C., Kaminski, H., Leinert, S., Breuer, L., Gladtke, D., Weber, S., and Kuhlbusch, T. A. J.: Contributions of carbonaceous particles from fossil emissions and biomass burning to PM_{10} in the Ruhr area, Germany, Atmos. Environ., 189, 174-186, https://doi.org/10.1016/j.atmosenv.2018.06.039, 2018.

Lack, D. A., and Langridge, J. M.: On the attribution of black and brown carbon light absorption using the Ångström exponent, Atmos. Chem. Phys., 13, 10535-10543, https://doi.org/10.5194/acp-13-10535-2013, 2013.

Laskin, A., Laskin, J., and Nizkorodov, S. A.: Chemistry of atmospheric brown carbon, Chem. Rev., 115, 4335-4382, https://doi.org/10.1021/cr5006167, 2015.

Liakakou, E., Kaskaoutis, D. G., Grivas, G., Stavroulas, I., Tsagkaraki, M., Paraskevopoulou, D., Bougiatioti, A., Dumka, U. C., Gerasopoulos, E., and Mihalopoulos, N.: Long-term brown carbon spectral characteristics in a Mediterranean city (Athens), Sci. Total Environ., 708, 135019, https://doi.org/10.1016/j.scitotenv.2019.135019, 2020.

Lin, Y. C., Tsai, C. J., Wu, Y. C., Zhang, R., Chi, K. H., Huang, Y. T., Lin, S. H., and Hsu, S. C.: Characteristics of trace metals in traffic-derived particles in Hsuehshan Tunnel, Taiwan: size distribution, potential source, and fingerprinting metal ratio, Atmos. Chem. Phys., 15, 4117-4130, https://doi.org/10.5194/acp-15-4117-2015, 2015.

Liou, K. N.: An introduction to atmospheric radiation, (2nd ed.p 583), New York: Academic press, Elsevier Science, 2002.

Massabò, D., Caponi, L., Bernardoni, V., Bove, M. C., Brotto, P., Calzolai, G., Cassola, F., Chiari, M., Fedi, M. E., Fermo, P., Giannoni, M., Lucarelli, F., Nava, S., Piazzalunga, A., Valli, G., Vecchi, R., and Prati, P.: Multi-wavelength optical determination of black and brown carbon in atmospheric aerosols, Atmos. Environ., 108, 1-12, https://doi.org/10.1016/j.atmosenv.2015.02.058, 2015.

Moreno, T., Querol, X., Alastuey, A., de la Rosa, J., Sánchez de la Campa, A. M., Minguillón, M., Pandolfi, M., González-Castanedo, Y., Monfort, E., and Gibbons, W.: Variations in vanadium, nickel and lanthanoid element concentrations in urban air, Sci. Total Environ., 408, 4569-4579, https://doi.org/10.1016/j.scitotenv.2010.06.016, 2010.

删除了：Li, M., Zhang, Q., Kurokawa, J. I., Woo, J. H., He, K., Lu, Z., Ohara, T., Song, Y., Streets, D. G., Carmichael, G. R., Cheng, Y., Hong, C., Huo, H., Jiang, X., Kang, S., Liu, F., Su, H., and Zheng, B.: MIX: a mosaic Asian anthropogenic emission inventory under the international collaboration framework of the MICS-Asia and HTAP, Atmos. Chem. Phys., 17, 935-963, https://doi.org/10.5194/acp-17-935-2017, 2017.

Norris, G., Duvall, R., Brown, S., and Bai, S.: EPA Positive Matrix Factorization (PMF) 5.0 Fundamentals and User Guide, available at: https://www.epa.gov/sites/production/files/2015-02/documents/pmf_5.0_user_guide.pdf (last access: September 2019), 2014.

Obregón, M. A., Serrano, A., Costa, M. J. and Silva, A. M.: Validation of libRadtran and SBDART models under different aerosol conditions, IOP Conf. Ser. Earth Environ. Sci., 28, 12010, https://doi.org/10.1088/1755-1315/28/1/012010, 2015.

Paatero, P., and Tapper, U.: Positive matrix factorization: A non-negative factor model with optimal utilization of error estimates of data values, Environmetrics, 5, 111-126, https://doi.org/10.1002/env.3170050203, 1994.

Paatero, P., Eberly, S., Brown, S. G. and Norris, G. A.: Methods for estimating uncertainty in factor analytic solutions, Atmos. Meas. Tech., 7(3), 781–797, https://doi:10.5194/amt-7-781-2014, 2014.

Pandey, A., Pervez, S., and Chakrabarty, R. K.: Filter-based measurements of UV–vis mass absorption cross sections of organic carbon aerosol from residential biomass combustion: Preliminary findings and sources of uncertainty, J. Quant. Spectrosc. Radiat. Transfer, 182, 296-304, https://doi.org/10.1016/j.jqsrt.2016.06.023, 2016.

Putaud, J. P., Van Dingenen, R., Alastuey, A., Bauer, H., Birmili, W., Cyrys, J., Flentje, H., Fuzzi, S., Gehrig, R., Hansson, H. C., Harrison, R. M., Herrmann, H., Hitzenberger, R., Hüglin, C., Jones, A. M., Kasper-Giebl, A., Kiss, G., Kousa, A., Kuhlbusch, T. A. J., Löschau, G., Maenhaut, W., Molnar, A., Moreno, T., Pekkanen, J., Perrino, C., Pitz, M., Puxbaum, H., Querol, X., Rodriguez, S., Salma, I., Schwarz, J., Smolik, J., Schneider, J., Spindler, G., ten Brink, H., Tursic, J., Viana, M., Wiedensohler, A., and Raes, F.: A European aerosol phenomenology – 3: Physical and chemical characteristics of particulate matter from 60 rural, urban, and kerbside sites across Europe, Atmos. Environ., 44, 1308-1320, https://doi.org/10.1016/j.atmosenv.2009.12.011, 2010.

Qin, Y. M., Tan, H. B., Li, Y. J., Li, Z. J., Schurman, M. I., Liu, L., Wu, C., and Chan, C. K.: Chemical characteristics of brown carbon in atmospheric particles at a suburban site near Guangzhou, China, Atmos. Chem. Phys., 18, 16409-16418, https://doi.org/10.5194/acp-18-16409-2018, 2018.

Qiu, C., Khalizov, A. F., Hogan, B., Petersen, E. L., and Zhang, R.: High sensitivity of diesel soot morphological and optical properties to combustion temperature in a shock tube, Environ. Sci. Technol., 48, https://doi.org/6444-6452, 10.1021/es405589d, 2014.

Rai, P., Furger, M., Slowik, J. G., Canonaco, F., Fröhlich, R., Hüglin, C., Minguillón, M. C., Petterson, K., Baltensperger, U., and Prévôt, A. S. H.: Source apportionment of highly time-resolved elements during a firework episode from a rural freeway site in Switzerland, Atmos. Chem. Phys., 20 (3), 1657–1674, https://doi.org/10.5194/acp-20-1657-2020, 2020.

Ricchiazzi, P., Yang, S., Gautier, C., and Sowle, D.: SBDART: A Research and Teaching Software Tool for Plane-Parallel Radiative Transfer in the Earth's Atmosphere, Bull. Amer. Meteorol. Soc., 79, 2101-2114, https://doi.org/10.1175/1520-0477(1998)079<2101:SARATS>2.0.CO;2, 1998.

Sandradewi, J., Prévôt, A. S. H., Szidat, S., Perron, N., Alfarra, M. R., Lanz, V. A., Weingartner, E., and Baltensperger, U.: Using aerosol light absorption measurements for the quantitative determination of wood burning and traffic emission contributions to particulate matter, Environ. Sci. Technol., 42, 3316-3323, https://doi.org/10.1021/es702253m, 2008.

Satheesh, S. K. and Srinivasan, J.: A method to estimate aerosol radiative forcing from spectral optical depths, J. Atmos. Sci., 63, 1082–1092, https://doi.org/10.1175/JAS3663.1, 2006.

Sheesley, R. J., Schauer, J. J., Garshick, E., Laden, F., Smith, T. J., Blicharz, A. P., and Deminter, J. T.: Tracking personal exposure to particulate diesel exhaust in a diesel freight terminal using organic tracer analysis, J. Exposure Sci. Environ. Epidemiol., 19, 172-186, https://doi.org/10.1038/jes.2008.11, 2009.

Tao, J., Zhang, L., Cao, J., and Zhang, R.: A review of current knowledge concerning $PM_{2.5}$ chemical composition, aerosol optical properties and their relationships across China, Atmos. Chem. Phys., 17, 9485-9518, https://doi.org/10.5194/acp-17-9485-2017, 2017.

Tasoglou, A., Saliba, G., Subramanian, R., and Pandis, S. N.: Absorption of chemically aged biomass burning carbonaceous aerosol, J. Aerosol Sci., 113, 141-152, https://doi.org/10.1016/j.jaerosci.2017.07.011, 2017.

Tian, J., Wang, Q., Ni, H., Wang, M., Zhou, Y., Han, Y., Shen, Z., Pongpiachan, S., Zhang, N., Zhao, Z., Zhang, Q., Zhang, Y., Long, X., and Cao, J.: Emission characteristics of primary brown carbon

absorption from biomass and coal burning: Development of an optical emission inventory for China, J. Geophys. Res.-Atmos., 124, 1879-1893, https://doi.org/10.1029/2018JD029352, 2019.

Tian, J., Wang, Q., Han, Y., Ye, J., Wang, P., Pongpiachan, S., Ni, H., Zhou, Y., Wang, M., Zhao, Y., and Cao, J.: Contributions of aerosol composition and sources to particulate optical properties in a southern coastal city of China, Atmos. Res., 235, 104744, https://doi.org/10.1016/j.atmosres.2019.104744, 2020.

Turpin, B. J. and Lim, H.-J.: Species contributions to $PM_{2.5}$ mass concentrations: Revisiting common assumptions for estimating organic mass, Aerosol Sci. Technol., 35(1), 602–610, https://doi.org/10.1080/02786820119445, 2001.

Wang, J., Ho, S. S. H., Ma, S., Cao, J., Dai, W., Liu, S., Shen, Z., Huang, R., Wang, G., and Han, Y.: Characterization of $PM_{2.5}$ in Guangzhou, China: uses of organic markers for supporting source apportionment, Sci. Total Environ., 550, 961-971, https://doi.org/10.1016/j.scitotenv.2016.01.138, 2016.

Wang, J., Nie, W., Cheng, Y., Shen, Y., Chi, X., Wang, J., Huang, X., Xie, Y., Sun, P., Xu, Z., Qi, X., Su, H., and Ding, A.: Light absorption of brown carbon in eastern China based on 3-year multi-wavelength aerosol optical property observations and an improved absorption Ångström exponent segregation method, Atmos. Chem. Phys., 18, 9061-9074, https://doi.org/10.5194/acp-18-9061-2018, 2018.

Wang, L., Li, Z., Tian, Q., Ma, Y., Zhang, F., Zhang, Y., Li, D., Li, K., and Li, L.: Estimate of aerosol absorbing components of black carbon, brown carbon, and dust from ground-based remote sensing data of sun-sky radiometers, J. Geophys. Res.-Atmos., 118, 6534-6543, https://doi.org/10.1002/jgrd.50356, 2013.

Wang, Q., Huang, R.-J., Cao, J., Tie, X., Shen, Z., Zhao, S., Han, Y., Li, G., Li, Z., Ni, H., Zhou, Y., Wang, M., Chen, Y. and Su, X.: Contribution of regional transport to the black carbon aerosol during winter haze period in Beijing, Atmos. Environ., 132, 11–18, https://doi.org/10.1016/j.atmosenv.2016.02.031, 2016.

Wang, Q., Cao, J., Han, Y., Tian, J., Zhu, C., Zhang, Y., Zhang, N., Shen, Z., Ni, H., Zhao, S., and Wu, J.: Sources and physicochemical characteristics of black carbon aerosol from the southeastern

Tibetan Plateau: internal mixing enhances light absorption, Atmos. Chem. Phys., 18, 4639-4656, https://doi.org/10.5194/acp-18-4639-2018, 2018a.

Wang, Q. Y., Cao, J. J., Han, Y. M., Tian, J., Zhang, Y., Pongpiachan, S., Zhang, Y. G., Li, L., Niu, X. Y., Shen, Z. X., Zhao, Z. Z., Tipmanee, D., Bunsomboonsakul, S., Chen, Y., and Sun, J.: Enhanced light absorption due to the mixing state of black carbon in fresh biomass burning emissions, Atmos. Environ., 180, 184-191, https://doi.org/10.1016/j.atmosenv.2018.02.049, 2018b.

Wang, Q., Han, Y., Ye, J., Liu, S., Pongpiachan, S., Zhang, N., Han, Y., Tian, J., Wu, C., Long, X., Zhang, Q., Zhang, W., Zhao, Z., and Cao, J.: High Contribution of Secondary Brown Carbon to Aerosol Light Absorption in the Southeastern Margin of Tibetan Plateau, Geophys. Res. Lett., 46, 4962-4970, https://doi.org/10.1029/2019GL082731, 2019a.

Wang, Q., Ye, J., Wang, Y., Zhang, T., Ran, W., Wu, Y., Tian, J., Li, L., Zhou, Y., Hang Ho, S. S., Dang, B., Zhang, Q., Zhang, R., Chen, Y., Zhu, C., and Cao, J.: Wintertime Optical Properties of Primary and Secondary Brown Carbon at a Regional Site in the North China Plain, Environ. Sci. Technol., 53, 12389-12397, 10.1021/acs.est.9b03406, 2019b.

Wang, Y. Q., Zhang, X. Y., and Draxler, R. R.: TrajStat: GIS-based software that uses various trajectory statistical analysis methods to identify potential sources from long-term air pollution measurement data, Environ. Modell. Softw., 24, 938-939, https://doi.org/10.1016/j.envsoft.2009.01.004, 2009.

Xie, M., Hays, M. D., and Holder, A. L.: Light-absorbing organic carbon from prescribed and laboratory biomass burning and gasoline vehicle emissions, Sci. Rep., 7, https://doi.org/10.1038/s41598-017-06981-8, 2017.

Xing, J., Shao, L., Zhang, W., Peng, J., Wang, W., Shuai, S., Hu, M., and Zhang, D.: Morphology and size of the particles emitted from a gasoline-direct-injection-engine vehicle and their ageing in an environmental chamber, Atmos. Chem. Phys., 20, 2781-2794, https://doi.org/10.5194/acp-20-2781-2020, 2020.

Xu, H. M., Cao, J. J., Ho, K. F., Ding, H., Han, Y. M., Wang, G. H., Chow, J. C., Watson, J. G., Khol, S. D., Qiang, J., and Li, W. T.: Lead concentrations in fine particulate matter after the phasing out of leaded gasoline in Xi'an, China, Atmos. Environ., 46, 217-224, https://doi.org/10.1016/j.atmosenv.2011.09.078, 2012.

Yang, M., Howell, S. G., Zhuang, J., and Huebert, B. J.: Attribution of aerosol light absorption to black carbon, brown carbon, and dust in China – interpretations of atmospheric measurements during EAST-AIRE, Atmos. Chem. Phys., 9, 2035-2050, https://doi.org/10.5194/acp-9-2035-2009, 2009.

Zanatta, M., Gysel, M., Bukowiecki, N., Müller, T., Weingartner, E., Areskoug, H., Fiebig, M., Yttri, K. E., Mihalopoulos, N., Kouvarakis, G., Beddows, D., Harrison, R. M., Cavalli, F., Putaud, J. P., Spindler, G., Wiedensohler, A., Alastuey, A., Pandolfi, M., Sellegri, K., Swietlicki, E., Jaffrezo, J. L., Baltensperger, U., and Laj, P.: A European aerosol phenomenology-5: Climatology of black carbon optical properties at 9 regional background sites across Europe, Atmos. Environ., 145, 346-364, https://doi.org/10.1016/j.atmosenv.2016.09.035, 2016.

Zhang, T., Cao, J. J., Tie, X. X., Shen, Z. X., Liu, S. X., Ding, H., Han, Y. M., Wang, G. H., Ho, K. F., Qiang, J., and Li, W. T.: Water-soluble ions in atmospheric aerosols measured in Xi'an, China: Seasonal variations and sources, Atmos. Res., 102, 110-119, https://doi.org/10.1016/j.atmosres.2011.06.014, 2011.

Zhao, Z., Cao, J., Chow, J. C., Watson, J. G., Chen, A. L. W., Wang, X., Wang, Q., Tian, J., Shen, Z., Zhu, C., Liu, S., Tao, J., Ye, Z., Zhang, T., Zhou, J., and Tian, R.: Multi-wavelength light absorption of black and brown carbon at a high-altitude site on the Southeastern margin of the Tibetan Plateau, China, Atmos. Environ., 212, 54-64, https://doi.org/10.1016/j.atmosenv.2019.05.035, 2019.

Zheng, H., Kong, S., Wu, F., Cheng, Y., Niu, Z., Zheng, S., Yang, G., Yao, L., Yan, Q., Wu, J., Zheng, M., Chen, N., Xu, K., Yan, Y., Liu, D., Zhao, D., Zhao, T., Bai, Y., Li, S., and Qi, S.: Intra-regional transport of black carbon between the south edge of the North China Plain and central China during winter haze episodes, Atmos. Chem. Phys., 19, 4499-4516, https://doi.org/10.5194/acp-19-4499-2019, 2019.

Zhong, M., and Jang, M.: Dynamic light absorption of biomass-burning organic carbon photochemically aged under natural sunlight, Atmos. Chem. Phys., 14, 1517-1525, https://doi.org/10.5194/acp-14-1517-2014, 2014.

Zhu, C.-S., Cao, J.-J., Hu, T.-F., Shen, Z.-X., Tie, X.-X., Huang, H., Wang, Q.-Y., Huang, R.-J., Zhao, Z.-Z., Močnik, G., and Hansen, A. D. A.: Spectral dependence of aerosol light absorption at an urban

and a remote site over the Tibetan Plateau, Sci. Total Environ., 590-591, 14-21, https://doi.org/10.1016/j.scitotenv.2017.03.057, 2017.

Zotter, P., Herich, H., Gysel, M., El-Haddad, I., Zhang, Y., Močnik, G., Hüglin, C., Baltensperger, U., Szidat, S., and Prévôt, A. S. H.: Evaluation of the absorption Ångström exponents for traffic and wood burning in the Aethalometer-based source apportionment using radiocarbon measurements of ambient aerosol, Atmos. Chem. Phys., 17, 4229-4249, https://doi.org/10.5194/acp-17-4229-2017, 2017.

Table 1. Summary of light absorption at different wavelengths (Abs(λ), λ = 370, 470, 520, 590, 660, and 880 nm) and Absorption Ångström Exponent (AAE) of different emission sources.

Parameter[a]	Average	Standard deviation
Abs(370) (Mm^{-1})	15.7	5.3
Abs(470) (Mm^{-1})	11.4	3.7
Abs(520) (Mm^{-1})	9.7	3.0
Abs(590) (Mm^{-1})	8.3	2.6
Abs(660) (Mm^{-1})	7.0	2.2
Abs(880) (Mm^{-1})	4.9	1.5
AAE_{total}	1.41	0.05
AAE_{ship}	1.06	0.03
$AAE_{biomass}$	1.75	0.06
$AAE_{vehicle}$	0.96	0.06

[a]AAE_{total} represents the AAE caused by total light-absorbing aerosols while AAE_{ship}, $AAE_{biomass}$, and $AAE_{vehicle}$ are AAE from ship emissions, biomass burning, and motor vehicle emissions, respectively.

Table 2. The average mass concentrations of $PM_{2.5}$, carbonaceous matter, water-soluble ions, inorganic elements, and organics during the campaign.

Types	Species	Average	Standard deviation
$PM_{2.5}$ ($\mu g\ m^{-3}$)		14.3	4.2
Carbonaceous matter ($\mu g\ m^{-3}$)	organic carbon	2.7	1.1
	elemental carbon	0.8	0.3
Water-soluble ions ($\mu g\ m^{-3}$)	Na^+	0.5	0.2
	NH_4^+	0.6	0.4
	K^+	0.2	0.1
	Mg^{2+}	0.05	0.02
	Ca^{2+}	0.2	0.1
	Cl^-	0.23	0.2
	NO_3^-	0.6	0.3
	SO_4^{2-}	3.5	1.2
Inorganic elements ($ng\ m^{-3}$)	Ti	13.1	9.7
	V	2.4	1.4
	Mn	5.1	2.7
	Fe	127.3	78.9
	Ni	1.1	0.6
	Cu	28.0	14.4
	Zn	16.6	11.1
	Br	2.6	2.0
Organics ($ng\ m^{-3}$)	hopanes	0.2	0.05

Figure Captions

Figure 1. Time series of hourly averaged light absorption at different wavelengths (Abs(λ), λ = 370, 470, 520, 590, 660, and 880 nm). The different types of horizontal lines represent the four clusters of air masses.

Figure 2. Light absorption fractions of BC, BrC, and MD in the total light-absorbing aerosols. BC = black carbon; BrC = brown carbon; MD = mineral dust.

Figure 3. (a) Contributions of the four sources to each species from the positive matrix factorization model and (b) the light absorption of primary aerosols from each source at different wavelengths ($Abs_{pri}(\lambda)$, λ = 370, 470, 520, 590, 660, and 880 nm) during the study.

Figure 4. Contribution of different sources to light absorption of primary aerosols in each three-day backward-trajectory cluster during the campaign at Sanya. The map was drawn using ArcGIS software. The base map is the World Topographic Map from © ESRI (Environmental Systems Research Institute, Inc.) (www.arcgis.com/home/item.html?id=30e5fe3149c34df1ba922e6f5bbf808f).

Figure 5. The light absorption (Abs(λ)) of light-absorbing carbonaceous (LAC) aerosols from ship emissions, traffic emissions, and biomass burning. The dash line is power law fit.

Figure 6. The source-specific mass absorption cross section (MAC) of black carbon (BC) and brown carbon (BrC) at different wavelengths. The MAC of uncoated BC particles at each wavelength are extrapolated from 7.5 $m^2\ g^{-1}$ at 550 nm (Bond and Bergstrom, 2006) by assuming an BC absorption Ångström exponent of 1.1.

Figure 7. Direct radiative effect (DRE) of light-absorbing carbonaceous (LAC) aerosols from biomass burning, ship emissions, and motor vehicle emissions. The error bar represents one standard deviation. ES, TOA, ATM represent the DRE at the Earth's surface, the top of the atmosphere, and in the atmosphere, respectively.

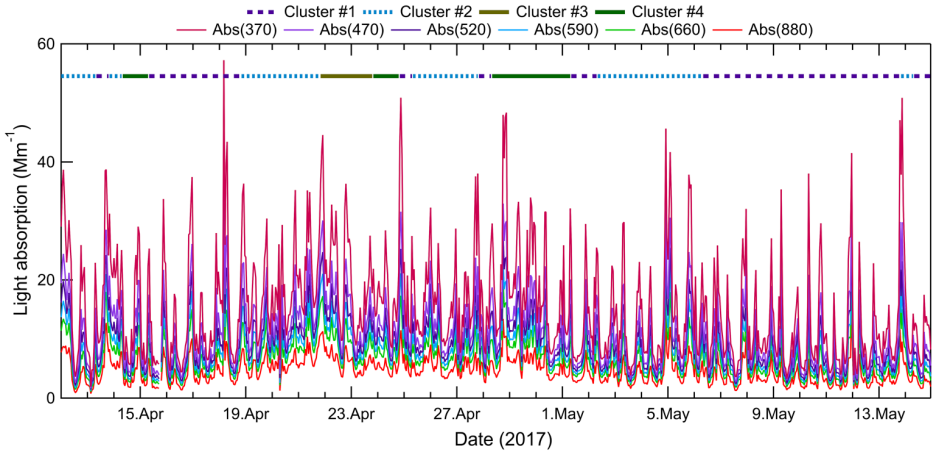
Cluster #1
Cluster #2
Cluster #3
Cluster #4
Abs(370)
Abs(470)
Abs(520)
Abs(590)
Abs(660)
Abs(880)
Light absorption (Mm-1)
60
40
20
0
15.Apr
19.Apr
23.Apr
27.Apr
1.May
5.May
9.May
13.May
Date (2017)

Figure 1.

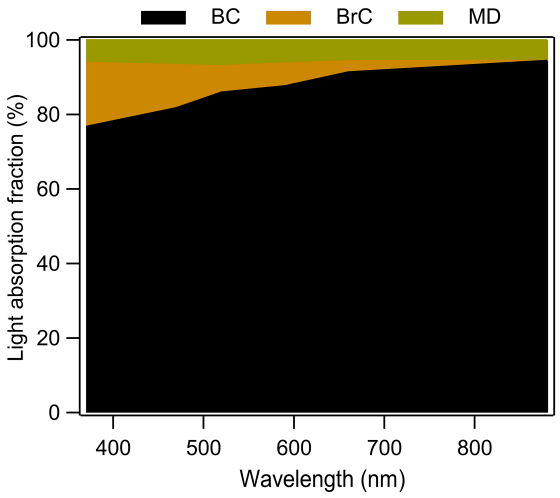
BC
BrC
MD
100
80
60
40
20
0
Light absorption fraction (%)
400
500
600
700
800
Wavelength (nm)

Figure 2.

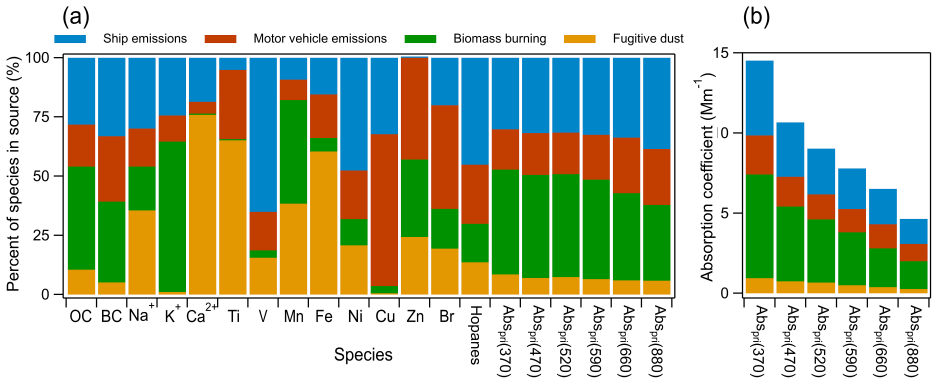
(a)
Ship emissions
Motor vehicle emissions
Biomass burning
Fugitive dust
Percent of species in source (%)
100
75
50
25
0
OC
BC
Na+
K+
Ca2+
Ti
V
Mn
Fe
Ni
Cu
Zn
Br
Hopanes
Abspr(370)
Abspr(470)
Abspr(520)
Abspr(590)
Abspr(660)
Abspr(880)
Species
(b)
Absorption coefficient (Mm-1)
15
0
5
0
Abspr(370)
Abspr(470)
Abspr(520)
Abspr(590)
Abspr(660)
Abspr(880)

Figure 3.

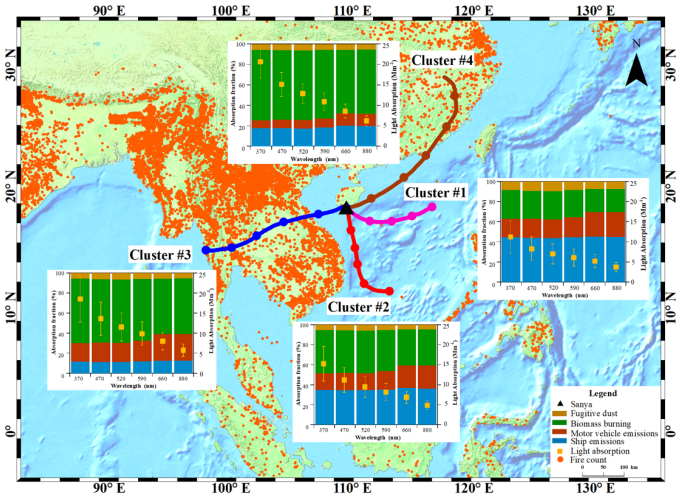
90° E
100° E
110° E
120° E
130° E
30° N
20° N
10° N
0°
N
Cluster #4
Cluster #1
Cluster #3
Cluster #2
Legend
Sanya
Fugitive dust
Biomass burning
Motor vehicle emissions
Ship emissions
Light absorption
Fire count
0
50
100 km

Figure 4.

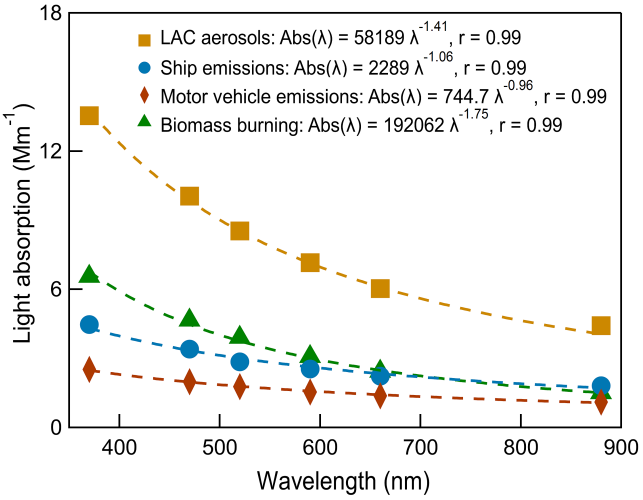
LAC aerosols: Abs(λ) = 58189 λ^-1.41, r = 0.99
Ship emissions: Abs(λ) = 2289 λ^-1.06, r = 0.99
Motor vehicle emissions: Abs(λ) = 744.7 λ^-0.96, r = 0.99
Biomass burning: Abs(λ) = 192062 λ^-1.75, r = 0.99
Light absorption (Mm^-1)
Wavelength (nm)
0
6
12
18
400
500
600
700
800
900

Figure 5.

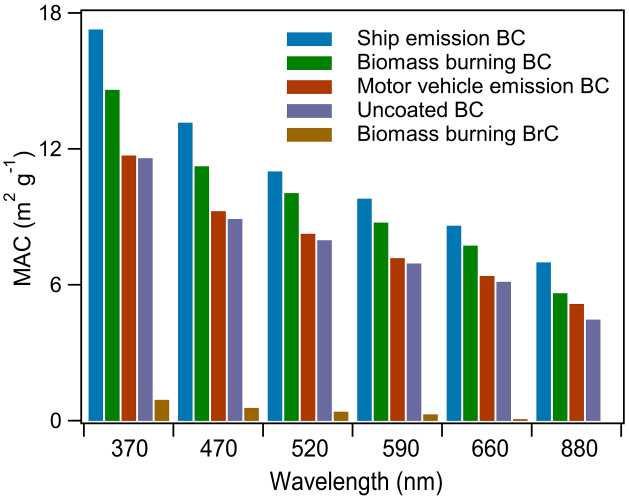
18
12
6
0
MAC (m^2 g^{-1})
Ship emission BC
Biomass burning BC
Motor vehicle emission BC
Uncoated BC
Biomass burning BrC
370
470
520
590
660
880
Wavelength (nm)

Figure 6.

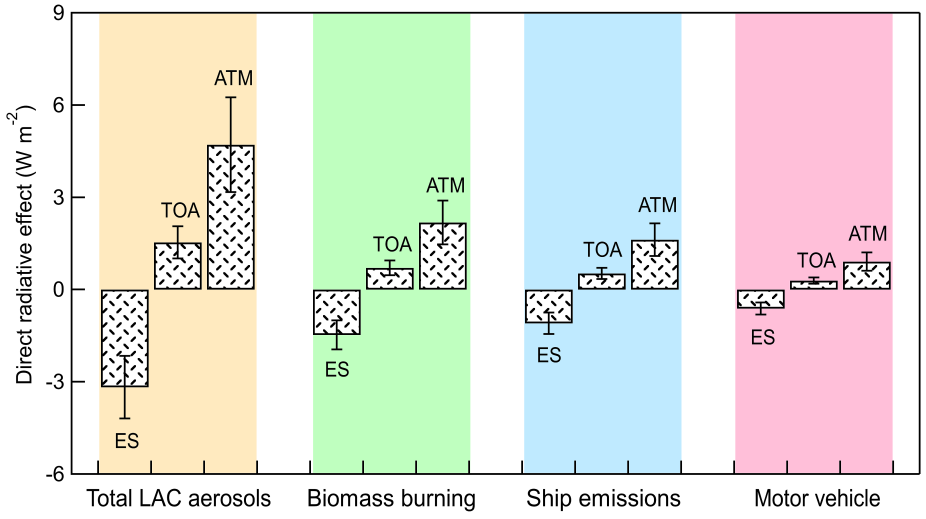
9
6
3
0
-3
-6
Direct radiative effect (W m-2)
ATM
TOA
ES
ATM
TOA
ES
ATM
TOA
ES
ATM
TOA
ES
Total LAC aerosols
Biomass burning
Ship emissions
Motor vehicle

Figure 7.